Quantum Entanglement of One-Dimensional Spinless Fermions

A Thesis Presented

by

Emanuel Casiano-Diaz

to

The Faculty of the Graduate College

of

The University of Vermont

In Partial Fullfillment of the Requirements

for the Degree of Master of Science

Specializing in Physics

May 2019

Defense Date: March 28th, 2019.

Thesis Examination Commitee:

Adrian Del Maestro, Ph.D, Advisor

Dennis Clougherty, Ph.D

Christopher Danforth, Ph.D, Chairperson

Cynthia J. Forehand, Ph.D, Dean of the Graduate College

Abstract

The constituents of a quantum many-body system can be inextricably linked, a phenomenon known as quantum entanglement. Entanglement can be used as a resource for quantum computing, quantum communication and detecting phase transitions, among others. The amount of entanglement can be quantified via the von Neumann and Rényi entropies, which have their origins in information theory.

In this work, the quantum entanglement between subsystems of a one dimensional lattice model of fermions is quantified. The von Neumann and Rényi entropies were calculated for two types of subsystems. In the first study, the subsystems were treated as two subsets of particles, and in the second, as two spatial subregions. Finally, by considering particle conservation rules, the amount of entanglement that can actually be accessed as a resource was calculated. In all cases, the quantum entanglement served to detect phase transitions in the model.

Acknowledgements

To my educators, for teaching me what I know today. To my incredible family for their never ending support. To my advisor, Adrian Del Maestro, for guiding my path as a graduate student and making the journey so enjoyable. And to Hatem Barghathi, for the countless hours that you spent teaching me about most of the topics that will be presented in this thesis and many more outside its scope.
Thanks.

This research was supported in part by the National Science Foundation under Award No. DMR-1553991. Computations were performed on the Vermont Advanced Computing Core supported in part by NSF award No. OAC-1827314.

Contents

Chapter 1

Introduction

1.1 The $t - V$ Model

So called "toy models" are ubiquitous in condensed matter physics. These describe a complex system in simple terms so that attention can be given to an underlying mechanism of such system. The Ising model, in it simplest form, can describe how a system spontaneously becomes a ferromagnet by considering interactions between quantum spins and tuning an external temperature. Similarly, the Hubbard model considers the interaction strength of electrons on a lattice and a hopping rate to describe the transition between conductor and insulator. The fact that the two aforementioned examples mention phase transitions is not mere coincidence.

Near a phase transition, small set of parameters governs macroscopical physical behavior, a phenomenon known as universality. Different systems having the same value for such universality parameters are said to fall under the same universality class.

The studies that will be presented in this thesis are concerned with a specific model, which shall be referred to as the $t-V$ model. This model, is equivalent to the XXZ spin model and describes N itinerant spinless fermions on a 1D lattice of size L. These fermions can tunnel to neighboring sites and the rate at which

they do so is proportional to a hopping parameter t. An interaction potential, V, between the fermions is also considered, which could be repulsive ($V > 0$) or attractive ($V < 0$). Periodic and anti-periodic boundary conditions will be assumed for the case of odd and even particles, respectively. Mathematically, this is represented by the following Hamiltonian:

$$H = -t \sum_i \left(c_i^\dagger c_{i+1} + c_{i+1}^\dagger c_i \right) + V \sum_i n_i n_{i+1} \tag{1.1}$$

where $c_i^\dagger$ (c_i) creates (annihilates) a fermion on site i and n_i counts the number of fermions on site i. Formally, these creation and annihilation operators are defined such that the following anticommutation relations are satisfied:

$$\left\{ c_i^\dagger, c_j^\dagger \right\} = 0 \ , \ \ \{c_i, c_j\} = 0 \ , \ \ \left\{ c_i, c_j^\dagger \right\} = \delta_{ij}, \tag{1.2}$$

where δ_{ij} is the Kronecker-Delta function. In the case that there exists a fermion on the site in which the creation operator acts, then $c^\dagger |1\rangle = |0\rangle$ in order to satisfy Pauli's Exclusion principle. The interaction term can then be understood conceptually as adding to the potential energy of the system if there are multiple particles in neighboring sites. Conceptually, the first term may be more difficult to understand in its current representation, due to this operator being non-diagonal. Nevertheless, expressing it in the momentum basis, where it is diagonal, illustrates that how contributions to the kinetic energy come from all particles with nonzero momentum (which will be all of them unless $t = 0$). A detailed mapping of the kinetic energy operator from lattice site to momentum basis can be seen in Appendix A.1.

Figure 1.1 shows the phase diagram of the $t - V$ model. For $V/t \ll -2$, the fermions cluster together due to the strong attractive interaction. The state in this regime is an equal superposition of all possible such cluster configurations over all lattice sites. At $V/t = -2$, the system undergoes a second order

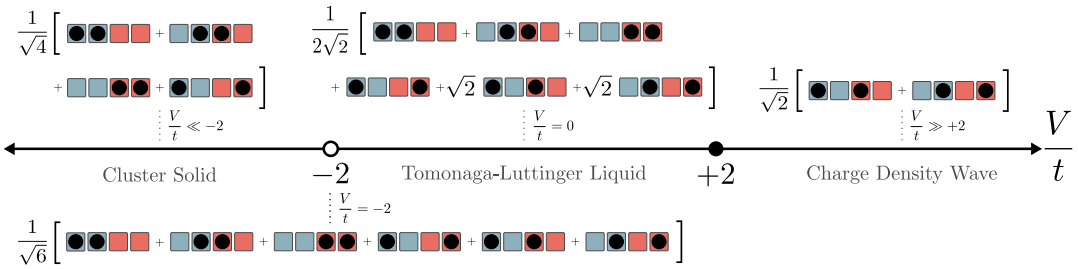

Figure 1.1: Phase diagram of the $t-V$ model accompanied by pictures of candidate ground states for $N = 2$ fermions on a $L = 4$ site lattice. For the purposes of measuring accessible entanglement, the lattice has been bipartitioned into spatial subregions A (blue) and B (red), each of size $\ell = 2$. We assume periodic boundary conditions. In the limit of strong attractive interactions where $V/t \ll -2$, the particles cluster together and there are L equally probable configurations corresponding to all translations of the cluster. At the first order phase transition where $V/t = -2$, all $\binom{L}{N}$ configurations are equally probable resulting in a flat state. In the TLL phase with $|V/t| < 2$, particles are delocalized and we have included a characteristic state corresponding to free fermions ($V = 0$). In the limit of strong repulsive interactions where $V/t \gg 2$, fermions maximize their distance from each other resulting in a charge density wave (CDW) phase. The open and closed circles on the V/t axis denote a first order and continuous phase transition, respectively.

phase transition into the Tomonaga-Luttinger Liquid (TLL) phase. Here, the state is in a superposition of all possible configurations of the fermions on the lattice, with the weights of each being different, in general. At $V/t = 2$, the system undergoes a continuous phase transition into the charged density wave (CDW) phase. At $V/t \gg 2$, the strong repulsion between particles leads to them forming an alternating pattern of particle-vacancy-particle- ... The state in this regime becomes an equal superposition of the only two possible such configurations.

Notice that in Figure 1.1 the lattice sites have two different colors, blue and red. This is to illustrate that a system can be partitioned into smaller subregions. In this particular example, each partition would be of size 2 lattice sites. In fact, subdividing a system into this smaller subsystems will be necessary for the main phenomenon of interest in this thesis: quantum entanglement. The bulk of this work will consist of quantifying the amount of entanglement of a

system via entropy measures. Before getting to explaining entanglement, in the next section, an overview of entropy or information measures will be given.

1.2 Information measures

The probabilistic nature of quantum mechanics, provides an ideal test bed for entropy measures. In section 1.1, it was mentioned that knowing something about A, will give you information about its entangled pair B. The amount of information gained in such measurement can be quantified by the entropy of a subsystem. Recall that, in essence, entropy is related to the disorder of a system. Thus, doing a measurement on a high entropy state, will give more information than in a highly ordered state, in which the outcome of the measurement is more like to be known a priori. For this reason, entropy measures will be referred to as information measures for the remainder of this work.

In the next section, the information measure used to quantify entanglement, will be introduced. Then, the actual measures of entanglement will be presented.

1.2.1 Shannon entropy

The Shannon or information entropy is the average amount of information gained from a a data set in which the entries occur according to some probability distribution. It is defined as:

$$S = -\sum_i p_i \log_b p_i \tag{1.3}$$

where the sum is carried over all entries in the data set and p_i is the probability of measuring entry i. The base b can be chosen arbitrarily depending on the context. The base will be chosen as the number e such that $\log_b \to \ln$ for the remainder of this work. Up next, a common day example will be presented in

order to give some intuition about how information gain can be estimated with Eq. (1.3)

Consider a regular coin flip. Disregarding all physical effects that can somehow bias the outcome, it is expected that either heads or tails will randomly occur with equal probability 1/2. Then, since there is no bias towards any of the two possible outcomes of the coin flip, the information gain should be at a maximum. The Shannon entropy for this case is:

$$\begin{aligned} S &= -\frac{1}{2}\ln\frac{1}{2} - \frac{1}{2}\ln\frac{1}{2} \\ &= \ln 2 \\ S &\approx 0.6931\ldots \end{aligned}$$

In base 2, this would correspond to a whole bit of information gained in the coin measurement. Now, consider a coin that has been modified in such a way that it is more likely to get one outcome than the other. For the sake of this example, let's say that heads shall occur with probability 2/3, while tails with 1/3. Then, since it is two times more likely that heads will occur instead of tails, more certainty about the outcome is known beforehand and thus the information gained decreases. Shannon entropy gives:

$$\begin{aligned} S &= -\frac{2}{3}\ln\frac{2}{3} - \frac{1}{3}\ln\frac{1}{3} \\ S &\approx 0.6365\ldots \end{aligned}$$

Finally, an extreme case would be a coin that was incorrectly manufactured and has heads on two sides. Opposite to a regular coin, in which maximum information is gained because both heads and tails have the same probability, the probability for heads to land in this case is 1, while 0 for tails. Since the result is already known before the coin flip, the information gain after the coin

flip is none. Shannon entropy gives:

$$S = -1 \ln 1 = 0$$

Now that some intuitive examples were discussed, the quantum information theory counterpart of Shannon's entropy will be presented.

1.2.2 von Neumann entropy

In calculating the Shannon entropy, the probabilities of random events occurring are required. The probabilities of finding a system in a certain state can be encoded in its density matrix. The density matrix is defined as:

$$\rho = |\Psi\rangle\langle\Psi| \tag{1.4}$$

where $|\Psi\rangle$ is the state of the full system, such that $|\Psi\rangle \in \mathcal{H} = A \otimes B$ and the normalization condition on the states of the system imply that $\operatorname{Tr}\rho = 1$. The state $|\Psi\rangle$ can be partitioned into subregions or subsystems that live in Hilbert Space A and B, respectively. The von Neumann entropy measures the information gained about subsystem B by doing a measurement on subsystem A. The von Neumann entropy is defined as:

$$S = -\operatorname{Tr}\rho_A \ln \rho_A \tag{1.5}$$

where ρ_A is known as the reduced density matrix of subsystem A and it is obtained by tracing out the degrees of freedom in B, an operation known as the partial trace (with respect to B, in this case). The reduced matrix of A is then:

$$\rho_A = \operatorname{Tr}_B \rho = \sum_b \langle\psi_b|\Psi|\psi_b\rangle \tag{1.6}$$

where the sum is carried over all possible states in which subsystem B can be in and ψ_b denotes each of these states. Normalization implies that $\mathrm{Tr}\,\rho_A = 1$.

The von Neumann requires access to the density matrix of the system. The density matrix can be obtained via exact diagonalization of the ground state Hamiltonian (see Appendix B.1 for details on Lanczos diagonalization). For large systems though, exact diagonalization is not feasible due to the exorbitant amount of memory required and quantum Monte Carlo (QMC) methods must be employed. In QMC methods, there is no access to the reduced density matrix, but the expectation value of a unitary operator that swaps the A states between two identical copies of a system gives higher powers of the reduced density matrix [1]. In other words, ρ_A is not accessible but ρ_A^α can be obtained for $\alpha > 1$. It was also shown experimentally [2] that ρ_A^α can be obtained by interference of two identical copies of ultra-cold atoms. Thus, a new formulation of the entropy must be introduced that depends on higher powers of ρ.

1.2.3 Rényi entanglement entropy

In order to calculate entropy via QMC or experimentally [1, 2], a measure that depends on powers of the reduced density matrix larger than 1 must be used, since these methods do not have access to the reduced density matrix. The Rényi entanglement entropy, which is the analogue of the Rényi entropy from information theory, provides an information measure that depends on ρ_A^α instead of ρ_A. The Rényi entanglement entropy is defined as:

$$S_\alpha = \frac{1}{1-\alpha} \ln \mathrm{Tr}\,\rho_A^\alpha \tag{1.7}$$

where α is known as the Rényi index. In the limit of $\alpha \to 1$, the Rényi entanglement entropy becomes to the von Neumann entropy. Higher Rényi indices will result in lower Rényi entanglement entropies, as shall be discussed up next.

Due to the normalization conditioned imposed on the reduced density matrix, the sum of its eigenvalues must also be unity. Each of the eigenvalues must then belong to the closed interval $[0, 1]$. Raising ρ_A to a power $\alpha > 1$ is equivalent to raising each eigenvalue by α and as a result, the trace of ρ_A will decrease. A lower trace of ρ_A will then make the Rényi entanglement entropy lower. Thus, S_α is a monotonically decreasing function of α.

Now that the $t - V$ model and the information measures have been introduced, it is time to discuss quantum entanglement itself.

1.3 Quantum entanglement

A quantum many body system is entangled if its constituents present correlations that cannot be classically described. Mathematically, a quantum many-body system is entangled if it cannot be factored into a tensor product of the state of subsystems A and B. The condition for entanglement is then,

$$|\Psi\rangle \neq |\Psi_A\rangle \otimes |\Psi_B\rangle \tag{1.8}$$

Assuming subsystems A and B are entangled with one another, knowing something about A automatically gives you some knowledge of B. Since the average information gained about B when measuring A can be quantified via von Neumann and Rényi entanglement entropies, these can be used as indication of how entangled the two subsystems are with each other. A system is highly entangled if its state possesses a large entanglement entropy.

The subsystems in which a system is partitioned can represent subsets of particles or quantum modes. The modes can represent spatial subregions, momenta, spins, etc... Since the case of entanglement in the $t - V$ model under a spatial bipartition was studied in this work, from here onwards, the mode partition shall be referred to as a spatial partition. Up next, an overview of

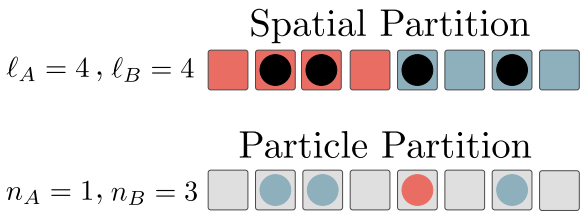

Figure 1.2: Schematic of a one-dimensional lattice of $L = 8$ sites and $N = 4$ particles under two types of bipartitions. The top lattice is bipartitioned into two spatial subregions A (red) and B (blue). The size of both subregions is $\ell_A = \ell_B = 4$ sites. The bottom lattice is bipartitioned into two subsets of identical particles. Subset A consists of only $n_A = 1$ particles, while B consists of $n_B = N - n_A = 3$.

particle-partitioned and spatially-partitioned entanglement is given.

A many-body system can be partitioned into subsets of particles. In the case of a particle bipartition, one of the subsets will have n particles and its complementary subset, $N-n$ particles, where N is the total number of particles in the system. To quantify entanglement between the subsets of particles, the $n-$body reduced density matrix ($n - RDM$) is used:

$$\rho_n = \int dx_{n+1} \cdots \int dx_N \langle x_{n+1} \dots x_N | \Psi \rangle \langle \Psi | x_{n+1} \dots x_N \rangle \tag{1.9}$$

where $|\Psi\rangle$ is the first quantized wavefunction of a system of N identical particles and it properly anti-symmetrized or symmetrized for fermions and bosons, respectively. The entanglement of a system under a particle bipartition allows to measure non-local effects, complementing the study of spatial entanglement. In measuring spatial entanglement, a system is bipartitioned into a spatial subregion of size ℓ_A and a complementary region size $L - \ell_A \equiv \ell_B$. Under this type of partition, states are represented in second quantization. In other words, a state $|\Psi\rangle = |n_1\rangle \otimes |n_2\rangle \cdots \otimes |n_N\rangle$ is characterized by the set of occupation numbers on each site. In the case of fermions, 0 and 1 correspond to a vacant and

occupied site, respectively. Figure 1.2 illustrates schematically a $1D$ lattice of size $L = 8$ and $N = 4$ under a spatial and then a particle bipartition.

1.3.1 Accessible Entanglement

Whether it's under a particle or spatial bipartition, the goal is to use the entanglement present in a system as a resource. The von Neumann and Rényi entropies provide mathematical quantification of the entanglement of a system. Nevertheless, for physical applications, superselection rules (SSR), such as particle number and spin conservation must be considered. An SSR, restricts the possible quantum states that can be obtained after measurement. For illustration of an SSR, take the example of N particles on a $1D$ lattice partitioned into two spatial subregions A and B. If initially there are n particles in the sites belonging to subregion A then, after measurement, the positions of the particles could change, but the number of particles in A will still be n. In this case, a local particle number SSR has been imposed. In Ref. [3], a new formulation for the entanglement was proposed that takes this particle number SSR into account.

For a quantum many-body system subject to physical laws conserving some quantity (particle number, charge, spin, etc.), the set of local operations on the state $|\Psi\rangle$ are limited to those that don't violate the corresponding global superselection rule. For simplicity, attention will be focused to the case of fixed total particles N and thus we are restricted to only those operators which locally preserve the particle number in A. The effect this has on the amount of entanglement that can be transferred to a qubit register is apparent from the simple example (adapted from Ref. [3] of one particle confined to two spatial modes A and B corresponding to site occupations. Then, for the state $|\Psi\rangle = (|1\rangle_A \otimes |0\rangle_B + |0\rangle_A \otimes |1\rangle_B)/\sqrt{2}$, Eq. (1.5) gives that $S_1 = \ln 2$. However, this entanglement cannot be transferred to a register prepared in initial state $|0\rangle_R$

via a SWAP gate:

$$\begin{aligned}
&\texttt{SWAP}\,|0\rangle_R \otimes (|1\rangle_A \otimes |0\rangle_B + |0\rangle_A \otimes |1\rangle_B)/\sqrt{2} \\
&= \frac{1}{\sqrt{2}}\left(|0\rangle_R \otimes \underbrace{|0\rangle_A \otimes |1\rangle_B}_{N=1} + |1\rangle_R \otimes \underbrace{|0\rangle_A \otimes |0\rangle_B}_{N\neq 1}\right)
\end{aligned}$$

The SWAP gate in the example above takes the register modes and exchanges them with the modes in subsystem A of the resource:

$$\texttt{SWAP}\,|\phi\rangle_R \otimes |\psi\rangle_A = |\psi\rangle_R \otimes |\phi\rangle_A \tag{1.10}$$

The SWAP can be defined such that it exchanges resource modes with modes in B instead. Notice that the first term post SWAP in the example preserves particle number in the resource, since there is a total of 1 particle in A and B. But, the last term is not physically allowed since it has no particles at all in A and B, thus violating the restriction that total particle number be fixed. The state of the register post-swap will remain in a product state, meaning that the amount of entanglement that can be accessed as a resource is identically zero. In general, it will be seen that the amount of accessible entanglement will be less or equal than the full entanglement of the system.

Formally, the accessible entanglement is defined as:

$$S_1^{\text{acc}} = \sum_n P_n S_1(\rho_{A_n}) \tag{1.11}$$

where the sum is carried over all possible local particle numbers of A, P_n is the probability that subsystem A will have n particles, S_1 is the von Neumann entropy, which will be a function of ρ_{A_n}. Notice the additional subscript n in the reduced density matrix expression. Whereas for the full entanglement entropy, knowing ρ_A would suffice, for the accessible entanglement entropy, the reduced density matrix must be also be projected onto the subspace of local

particle number n. Additionally, recall that the normalization condition asks for $\sum_n P_n = 1$. This accessible entropy was originally only well defined for the von Neumann entropy S_1. Recently, a generalized version of the accessible entanglement that works for Rényi indices greater than 1 was proposed [4], such that any accessible Rényi entropy can now be calculated.

Now that all the ground work for the results presented in this thesis has been introduced, an outline of the remaining chapters is given. In chapter 2, the particle-partitioned entanglement entropies in the $t-V$ model will be studied. By neglecting the exact entanglement entropies of free fermions, the contribution to particle entanglement coming from particle interactions is calculated. It is also seen that results from exact diagonalization agree with predictions coming from Tomonaga-Luttinger Liquid (TLL) theory. Chapter 3 will present computational results that support the generalization of the accessible Rényi entropies, this time under spatial bipartitions of the $t-V$ model. A power-law scaling is suggested for a peak near the continuous phase transition of the model. Then, the difference between full and accessible entanglement entropies is computed at various regimes of the model and it is shown that the probability of finding a number of particles n in one subregion of the system after measurement follows a Gaussian distribution in the TLL regime. Finally, chapter 4 will briefly discuss some unanswered questions that have emerged from the projects presented here and future ones will be discussed and a thesis summary is provided.

Chapter 2

Particle Partition Entanglement in the tV Model

2.1 Abstract

We investigate the scaling of the Rényi entanglement entropies for a particle bipartition of interacting spinless fermions in one spatial dimension. In the Tomonaga-Luttinger liquid regime, we calculate the second Rényi entanglement entropy and show that the leading order finite-size scaling is equal to a universal logarithm of the system size plus a non-universal constant. Higher-order corrections decay as power-laws in the system size with exponents that depend only on the Luttinger parameter. We confirm the universality of our results by investigating the one dimensional $t-V$ model of interacting spinless fermions via exact-diagonalization techniques. The resulting sensitivity of the particle partition entanglement to boundary conditions and statistics supports its utility as a probe of quantum liquids.

2.2 Introduction

Identical particles are fundamentally indistinguishable in quantum mechanics, unlike their classical counterparts that can always be discriminated due to an infinite set of observable properties. While this indistinguishability allows for the power provided by the second quantization formalism, it can also lead to ambiguity [5–7] when considering another defining property of composite quantum systems: entanglement. A pure state representing N quantum particles $|\Psi\rangle \in \mathcal{H}$ in Hilbert space $\mathcal{H}$ is said to be bipartite entangled if it cannot be written in a simple tensor product form $|\Psi\rangle \neq |\Psi_A\rangle \otimes |\Psi_B\rangle$ where A and B are vector spaces with $|\Psi_A\rangle \in A$ and $|\Psi_B\rangle \in B$ such that $A \otimes B = \mathcal{H}$. Conventionally, A and B correspond to a set of distinguishable single-particle modes whose occupation numbers are physical observables, i.e., spatial or momentum modes. However, for indistinguishable itinerant particles, there is no natural tensor product decomposition into single-particle modes due to the symmetrization or anti-symmetrization of the wavefunction with respect to the interchange of first quantized particle coordinates for bosons and fermions, respectively. Thus, the *mode entanglement* may depend on the choice of single-particle modes, leading to questions as to which (if any) are preferred and moreover, if these quantum correlations are even physically meaningful [3, 8–14]. For example, even in the absence of interactions, a system of N free itinerant bosons [15, 16] or fermions [17–19] is always entangled under a spatial biparition as a result of all allowed states being normalized linear combinations of Slater determinants or permanents.

Insights into these issues can be gained by considering the N-body wavefunction in first quantized form where a bipartition can be made in terms of identical particle labels. The resulting *n-particle partition entanglement* is a measure of quantum correlations between the subsets of n and $N-n$ particles. As individual (or groups of) identical particles are not operationally distin-

guishable, there have been claims that this type of entanglement is not useful as a resource for quantum information processing [8, 13, 20]. However, schemes have been recently proposed to transfer it to experimentally addressable modes [21]. In a foundational series of papers, Haque *et al.* explored the particle partition entanglement in fractional quantum hall [22, 23] and itinerant bosonic, fermionic and anyonic lattice gases in one spatial dimension [24, 25]. This type of particle partition entanglement has since been investigated in other one dimensional systems including the fermionic Calogero-Sutherland [26], anyonic hard-core [27] and bosonic Lieb-Liniger [28, 29] models as well as rotating bose and fermi gases in two dimensions [30]. In analogy to the universal finite size scaling behavior of the entanglement entropy of one dimensional quantum gases under a spatial mode bipartition [31–33], a leading order scaling form for the particle partition entanglement entropy S supported by exact diagonalization on small lattice models was proposed in Ref. [24] which is linear in the subsystem size n and logarithmic in the system size N: $S \sim n \ln N$.

Motivated by this empirical prediction, in this paper, we investigate the particle partition entanglement for itinerant interacting spinless fermions in one spatial dimension. For Galilean invariant systems in the spatial continuum, we confirm the scaling form proposed in Ref. [24] within the Tomonaga-Luttinger liquid framework [34, 35] and determine how the leading order power-law corrections to the asymptotic scaling depend on the strength of the interactions between particles for $n = 1$. By exploiting symmetries of the n-particle reduced density matrix, we are able to measure the particle entanglement entropy in the one dimensional fermionic $t - V$ model for systems composed of up to $M = 28$ lattice sites at half filling, allowing us to confirm our predictions from continuum field theory.

The rest of this paper is organized as follows. We introduce a quantitative measure of entanglement, the Rényi entanglement entropy and discuss some known results for interacting spinless fermions. We then derive the 1-particle

entanglement entropy in the low energy limit and compare with exact diagonalization results on a lattice. We conclude with a discussion of the role of boundary conditions, degeneracy and implications for future studies of models with generalized statistics. All numerical data and code necessary to reproduce the results and figures in this paper can be found in Ref. [36].

2.3 Particle Partition Entanglement

The entanglement of the pure state $\left|\Psi\right\rangle$ under a general bipartition into A and B can be quantified via the Rényi entanglement entropy:

$$S_\alpha\left[\rho_A\right] \equiv \frac{1}{1-\alpha}\ln\left(\mathrm{Tr}\rho_A^\alpha\right), \tag{2.1}$$

where α is the Rényi index and ρ_A is the reduced density matrix obtained by tracing out all degrees of freedom in B

$$\rho_A \equiv \mathrm{Tr}_B\left|\Psi\right\rangle\left\langle\Psi\right|. \tag{2.2}$$

For $\alpha = 1$ the Rényi entropy is equivalent to the von Neumann entropy: $-\mathrm{Tr}\ \rho_A \ln \rho_A$.

While it is common for A and B to be defined by some set of observable modes, for a many-body system consisting of N itinerant particles they can refer to subsystems of particles. As depicted in Fig. 2.1, such a bipartition of indistinguishable particles (in this case spinless fermions) is completely specified by the number of particles in the subsystem, n. The entanglement entropy under a particle bipartition is then a function of the familiar n-body reduced density matrix ρ_n, (n-RDM) defined in first quantized notation in one spatial dimension as:

$$\rho_n \equiv \int dx_{n+1}\cdots\int dx_N \left\langle x_{n+1}\cdots x_N|\Psi\right\rangle\left\langle\Psi|x_{n+1}\cdots x_N\right\rangle \tag{2.3}$$

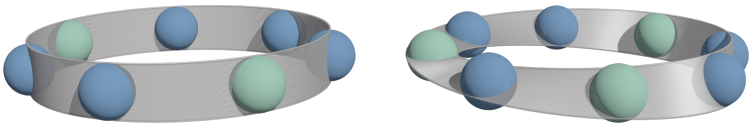

periodic: $N = 7,\ n = 2$ anti-periodic: $N = 8,\ n = 3$

Figure 2.1: A schematic of $N = 7$ fermions in one spatial dimension subject to periodic boundary conditions under a n-particle partition with $n = 2$ (left) and anti-periodic boundary conditions with $N = 8$ and $n = 3$ (right). All fermions are identical, while the partitions A and B are distinguished via their first quantized labels.

where we have taken the normalization $\mathrm{Tr}\rho_n = 1$. From this form, it is clear that the particle partition Rényi entropies $S_\alpha[\rho_n] \equiv S_\alpha(n)$ only vanish when the N-body ground state $\left|\Psi\right\rangle$ can be written as a general tensor product state in first quantized notation. This immediately implies that $S_\alpha(n) = 0$ when all particles are condensed into a single mode, and thus the particle partition entanglement of the non-interacting Bose gas is identically zero, in contrast to non-zero results for its spatial mode entanglement [15, 16]. This is not the case for many-fermion systems, which always have non-zero particle entanglement, even in the absence of interactions [18]. Particle entanglement entropy is sensitive to both interactions and statistics, and as ρ_n is free of any length scale, it can capture non-local effects making it complimentary to the more conventionally studied spatial mode entanglement entropy.

As described in the introduction, Zozulya et al. [24] first proposed a "standard" finite-size scaling form for the particle entanglement entropy of fermions:

$$S(n, N) = \ln \binom{N}{n} + a + \mathcal{O}\left(\frac{1}{N^\gamma}\right) \tag{2.4}$$

where a and γ are non-universal dimensionless numbers that can depend on n. These coefficients are known for the case of non-interacting fermions where $a = 0$ [25] and for the Laughlin state with filling fraction ν: $a = -n \ln \nu$, $\gamma = 2$ when $n \ll N$ [22].

Recently, a general scaling form like Eq. (2.4) was investigated for a sys-

tem of interacting bosons in the spatial continuum with $n = 1$ [29] where it was found that the pre-factor of the leading order logarithm is non-universal, depending on the interaction strength. In this paper, we apply extensions of these methods to interacting Galilean invariant one dimensional fermions and are able to systematically derive Eq. (2.4) while presenting results for both a and γ as a function of the interaction strength.

2.4 One-particle entanglement in fermionic Tomonaga-Luttinger liquids

We are interested in the asymptotic finite size scaling of the entanglement entropy (EE) as defined in Eq. (2.1) which can be investigated for any Rényi index α. Here we focus on the special case of $\alpha = 2$ as (i) the calculation will turn out to be analytically tractable and (ii) as it can be related to the expectation value of a local observable, it has proved to be the most direct numerical [1, 37–39] and even experimental [2, 40] route to its measurement. We begin by considering a system of N one-dimensional interacting spinless fermions with density $\rho_0 = N/L$ (where L is the length of the system) whose low energy properties can be described in terms of the universal quantum hydrodynamics of Tomonaga-Luttinger liquid (TLL) theory [34, 35]. Within this framework, at zero temperature in the thermodynamic limit, any n-body reduced density matrix can in principle be computed [41] and in particular for $n = 1$ [42]

$$\rho_1(x, x') = \frac{\sin(\pi\rho_0|x - x'|)}{\pi\rho_0 L|x - x'|(1 + |x - x'|^2\Lambda^2)^{(K+K^{-1}-2)/4}}, \tag{2.5}$$

where $\mathrm{Tr}\,\rho_1 = 1$ and both the ultraviolet (inverse short-distance) cutoff Λ and TLL parameter K depend on the microscopic details of the interaction between particles. Specifically, K characterizes the nature of the interaction, where $0 < K < 1$ ($K > 1$) corresponds to repulsive (attractive) interactions with free

fermions having $K = 1$. For ease of notation, we will replace the non-negative K-dependent exponent in Eq. (2.5) with $g \equiv (K + K^{-1} - 2)/4$.

The one-particle partition second Rényi entanglement entropy can be computed by using ρ_1 in Eq. (2.1)

$$\begin{aligned} S_2(n=1) = -\ln\left(\mathrm{Tr}\left[\rho_1^2\right]\right) &= -\ln\left(\int_{-L/2}^{L/2} dx \int_{-L/2}^{L/2} dx' \rho_1(x,x')\,\rho_1(x',x)\right) \\ &= \ln(N) - \ln(f(N,g,\Lambda/\rho_0)), \end{aligned} \tag{2.6}$$

where we have used translational invariance of the system and

$$\begin{aligned} f(N,g,\Lambda/\rho_0) = &\int_0^\infty dy \frac{2\sin^2(\pi y)}{\pi^2 y^2 (1+y^2\Lambda^2/\rho_0^2)^{2g}} \\ &- \int_{N/2}^\infty dy \frac{2\sin^2(\pi y)}{\pi^2 y^2 (1+y^2\Lambda^2/\rho_0^2)^{2g}}. \end{aligned} \tag{2.7}$$

The first integral can be evaluated exactly in terms of special functions:

$$\begin{aligned} A(g,\Lambda/\rho_0) &= \int_0^\infty dy \frac{2\sin^2(\pi y)}{\pi^2 y^2 (1+y^2\Lambda^2/\rho_0^2)^{2g}} \\ &= \frac{\pi^{4g+\frac{1}{2}} \rho_0^{4g} \sec(2\pi g)\, {}_1F_2\left(2g; 2g+1, 2g+\frac{3}{2}; \pi^2\Lambda^{-2}\rho_0^2\right)}{2\Lambda^{4g}\Gamma(2g+1)\Gamma(2g+\frac{3}{2})} \\ &\quad + \frac{\Lambda\Gamma\left(2g+\frac{1}{2}\right)\left[{}_1F_2\left(-\frac{1}{2}; \frac{1}{2}, \frac{1}{2}-2g; \pi^2\Lambda^{-2}\rho_0^2\right) - 1\right]}{\pi^{3/2}\rho_0\Gamma(2g)}. \end{aligned} \tag{2.8}$$

where ${}_1F_2(q;c,d;z)$ is the generalized hypergeometric and $\Gamma(z)$ the Gamma function. The leading order N dependence of the second integral in Eq. (2.7) can be extracted by replacing the highly oscillating periodic function $\sin^2(\pi y)$, in the large N limit, by its average over one period, i.e., $\sin^2(\pi y) \approx 1/2$ and expanding the rest of the integrand for large y. We find

$$f(N,g,\Lambda/\rho_0) \simeq A(g,\Lambda/\rho_0) - \frac{2^{4g+1}}{\pi^2(4g+1)(\Lambda/\rho_0)^{4g}} \frac{1}{N^{4g+1}} \tag{2.9}$$

and thus the second Rényi EE for $n = 1$ has the asymptotic form

$$S_2(n=1) = \ln(N) - \ln\left[A(g, \Lambda/\rho_0)\right] + \frac{b(g, \Lambda/\rho_0)}{N^{4g+1}} + \mathcal{O}\left(\frac{1}{N^{4g+2}}\right) \tag{2.10}$$

where

$$b(g, \Lambda/\rho_0) = \frac{2^{4g+1}}{\pi^2(4g+1)(\Lambda/\rho_0)^{4g} A(g, \Lambda/\rho_0)}. \tag{2.11}$$

This result constitutes an analytical confirmation of the empirical scaling form in Eq. (2.4) first proposed by Haque *et al.* [24, 25], with $n = 1$, where

$$a = -\ln\left[A(g, \Lambda/\rho_0)\right], \ \gamma = 4g + 1. \tag{2.12}$$

2.4.1 Non-interacting spinless fermions

In the non-interacting limit when $K = 1$ ($g = 0$), Eq. (2.8) yields $A(0, \Lambda/\rho_0) = 1$ and thus $a = 0$ in agreement with previous calculations of the particle partition EE for free fermions (FF) on a lattice [24] where it was found that $S_{2,FF}(n = 1) = \ln N$. However, combining Eqs. (2.10)-(2.11) for $g = 0$ yields

$$S_2(n=1) \simeq \ln(N) + \frac{2}{\pi^2 N}. \tag{2.13}$$

in disagreement with the lattice result by a factor of $\mathcal{O}(N^{-1})$. To ensure that this discrepancy does not arise from the approximations made in expanding the integral in Eq. (2.7) we can return to the exact expression for the 1-RDM for non-interacting spinless fermions:

$$\rho_{1,FF}\left(x, x'\right) = \frac{\sin(\pi\rho_0|x - x'|)}{\pi\rho_0 L|x - x'|}, \tag{2.14}$$

which leads to a soluble integral and analytic form for the EE in the spatial continuum:

$$S_{2,FF}(n=1) = \ln(N) - \ln\left\{\frac{2\left[N\pi \mathrm{Si}(N\pi) + \cos(\pi N) - 1\right]}{\pi^2 N}\right\} \tag{2.15}$$

where $\mathrm{Si}(z)$ is the sine integral. Expanding for large N recovers the asymptotic form in Eq. (2.13) which differs from the known lattice result.

2.4.2 Effects of boundary conditions

The origin of this $1/N$ difference between free spinless fermions in the continuum vs. the lattice is related to our neglect of finite-size boundary conditions when studying the asymptotic behavior of the second Rényi EE. To properly capture the finite-size effects of periodic boundary conditions we replace separations $|x - x'|$ with the chord length between two points on a ring of circumference L [43]:

$$|x - x'| \to \frac{L}{\pi} \sin\left(\frac{\pi}{L}|x - x'|\right). \tag{2.16}$$

Using the finite-size corrected 1-RDM, the integral in Eq. (2.7) takes the form

$$f(N, g, \Lambda/\rho_0) = \frac{2}{N^2}\int_0^{N/2} dy \frac{\sin^2(\pi y)}{\sin^2(\frac{\pi y}{N})\left[1 + \frac{N^2\Lambda^2}{\pi^2\rho_0^2}\sin^2(\frac{\pi y}{N})\right]^{2g}}. \tag{2.17}$$

where the effects of finite L will appear only in the prefactors of decaying terms in an asymptotic expansion. Employing Eq. (2.17) for free fermions with $g = 0$ we recover the known lattice result $S_{2,FF}(n=1) = \ln(N)$. For all subsequent comparisons with numerical data at finite g we employ the appropriately finite size corrected form of the 1-RDM when computing the Rényi entanglement entropy.

2.5 Exact diagonalization of the $t-V$ chain of spinless fermions

In order to test the validity of our main result in Eq. (2.10) for the $n = 1$ particle partition EE, we consider the $t-V$ model of N spinless fermions on a chain with M sites defined by the Hamiltonian

$$H = -t \sum_i \left(c_i^\dagger c_{i+1} + c_{i+1}^\dagger c_i \right) + V \sum_i n_i n_{i+1} \tag{2.18}$$

where $c_i^\dagger$ and c_i are the fermionic creation and annihilation operators at site i and $n_i = c_i^\dagger c_i$ is the occupation number. The model is parameterized by the nearest-neighbor hopping amplitude $t > 0$, and interaction strength V. We consider only the half-filled case ($M = 2N$) with periodic boundary conditions (PBC) for odd number of fermions N, while for even N we use antiperiodic boundary conditions (APBC) to avoid the otherwise degenerate ground state [43] (See Fig. 2.1). In order to make connection with the general TLL theory described above, we require a method to determine the parameter K from the microscopic $t-V$ model. This can be accomplished via the Jordan–Wigner transformation [44] which maps the $t-V$ model onto the XXZ spin-1/2 chain that is exactly solvable [45, 46]. In the range $|V/t| < 2$, the system is known to be in the TLL phase, where the analytical form of K is given by

$$K = \frac{\pi}{2\cos^{-1}(-V/2t)}. \tag{2.19}$$

By increasing the repulsive interaction across $V/t = 2$ ($K = 1/2$), the system undergoes a continuous phase transition to a charge-density wave (CDW) phase. In contrast, the transition across $V/t = -2$ ($K \to \infty$) is a discrete one, where the fermions tend to form a single cluster.

Beginning with the non-interacting case ($V/t = 0$), the free fermionic Hamil-

tonian is diagonal in the momentum-space representation leading to a ground state that is a Slater determinant of the N lowest energy modes. The rank of the resulting n-RDM is $\binom{N}{n}$ and with equal eigenvalues [24], it follows (as introduced above) that all the Rényi EEs are equal to

$$S_{\alpha,FF}(n) = \ln \binom{N}{n}. \tag{2.20}$$

In the presence of interactions, we calculate the von Neumann ($\alpha = 1$) and the second ($\alpha = 2$) Rényi EEs from the ground state of Eq. (2.18) which we obtain via numerical exact diagonalization. The resulting n-RDM has maximum possible rank $\binom{M}{n}$ due to the indistinguishability of the $n < N$ particles in the partition, as opposed to $n!\binom{M}{n}$, the full dimension of the Hilbert space in the first quantized basis. Exploiting this symmetry, (for details, see **??**) we are able to study systems up to $M = 28$ sites, a considerable advancement over previous work [25]. The results are shown in Fig. 2.2 which demonstrates that the entanglement entropy $S_\alpha(n = 1)$ increases with increasing interaction strength $|V/t|$ up to a maximum of $S_{\alpha,FF}(n = 1) + \ln 2$ (for even N) in the limit $|V/t| \to \infty$ [24, 25]. For attractive interactions, $S_\alpha(n = 1)$ displays a sharp increase around the first-order transition point $V/t = -2$. In contrast, $S_\alpha(n = 1)$ does not seem to be sensitive to the continuous transition at $V/t = 2$ [24]. However, when considering a macroscopic partition size $n = N/2$, we observe that $S_\alpha(n = N/2)$ develops a peak near $V/t = 2$ which appears to approach the critical point as we increase N (Fig. 2.2 (b)). Eventually, $S_\alpha(n = N/2)$ saturates to $\ln \binom{N}{N/2} + \ln 2$ in the limit $V/t \to \infty$, with details given in C.2.

We now turn to the TLL region $|V/t| < 2$, where we expect the scaling of the interaction contribution to the EE: $S_2(n = 1) - \ln(N)$, to be linear in $1/N^{4g+1}$ with corrections of $\mathcal{O}(1/N^{4g+2})$ as in Eq. (2.10). To test this prediction, we

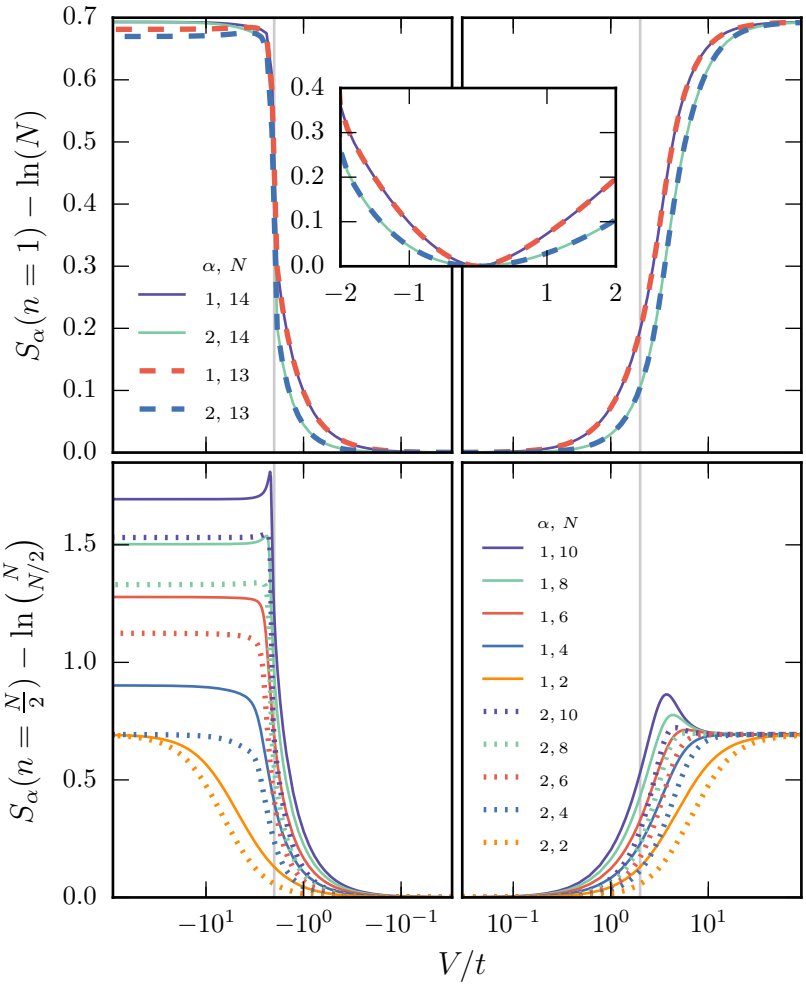

Figure 2.2: Interaction effects on the n-particle entanglement entropy $S_\alpha(n)$ for $\alpha = 1, 2$ in the ground state of the $t - V$ model. (a) $S_\alpha(n = 1) - \ln N$ vs V/t for $N = 13$ and 14 with periodic and anti-periodic boundary conditions, respectively. The light gray vertical lines mark the location of the known phase transitions at $V/t = \pm 2$. The subtracted $\ln(N)$ term is the one-particle entanglement entropy for free fermions. Inset: the Tomonaga-Luttinger liquid region where we expect the continuum theory to apply. (b) $S_\alpha(n = N/2) - \ln\binom{N}{N/2}$ vs V/t for *macroscpic* partitions with $1 \leq n \leq 5$ and anti-periodic boundary conditions. As $n \to N/2$, features appear near the phase transitions for $\alpha = 1$.

rearrange Eq. (2.10) as:

$$\frac{S_2(n=1) - \ln(N) - a}{b} = N^{-(4g+1)} + \mathcal{O}\left(N^{-(4g+2)}\right). \tag{2.21}$$

and calculate $S_2(n = 1)$ as a function of N using the ground state of $t - V$ model for different values of the interaction strength V/t, deep in the TLL

phase (away from the phase transitions). For each interaction strength V/t, we compute $g = (K + K^{-1} - 2)/4$ using Eq. (2.19) and extract a and b from a linear fit to the $S_2(n = 1) - \ln(N)$ vs $N^{-(4g+1)}$ data set. Next, we use the extracted coefficients to rescale $S_2(n = 1) - \ln(N)$ according to Eq. (2.21). The results are illustrated in Fig. 2.3, where, for suitably large N, the data follows the straight line predicted by Eq. (2.21) with unit slope, verifying the TLL scaling form in Eq. (2.10). Deviations from linearity for smaller N arise due to finite size corrections of $\mathcal{O}(1/N^{4g+2})$.

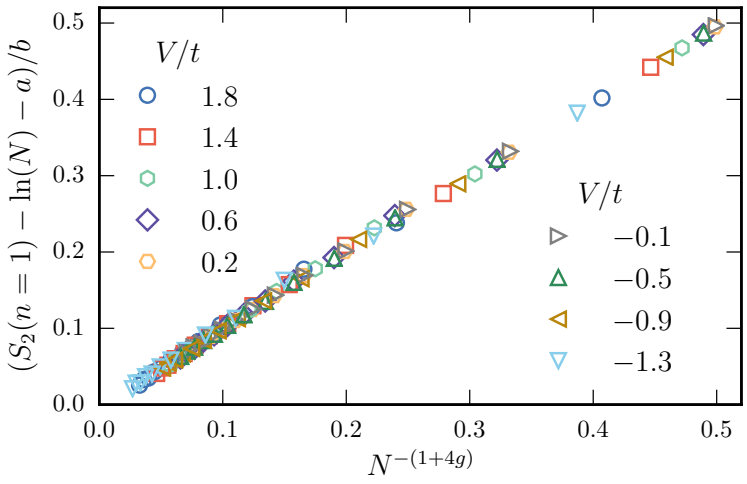

Figure 2.3: Finite size scaling of $S_2(n = 1) - \ln(N)$ with $N^{-(4g+1)}$ for $2 \leq N \leq 14$ confirming the empirical asymptotic scaling predicted by Zozulya *et al.* [22] and identifying the power of the leading finite size correction as $\gamma = 4g + 1$. The coefficients a and b depend on the interaction strength V/t and are calculated from a linear fit of the exact diagonalization data according to Eq. (2.10).

Having understood the asymptotic scaling of the 1-particle partition Rényi EE with N, we now consider its dependence on the interaction strength g. This amounts to asking if the g-dependence of the scaling coefficients a and b for the $t - V$ model can be predicted from our continuum theory. To answer this question we calculate the second Rényi EE for $|V/t| < 2$ in the liquid phase at fixed N by evaluating the full integral in Eq. (2.17) numerically including all contributions from finite N. However, in order to compare the resulting particle EE with that obtained from the exact diagonalization, we need to identify the

corresponding non-universal value of the ratio Λ/ρ_0 in the $t-V$ model. At half filling, the average particle density is $\rho_0 = 1/2x_0$ where x_0 is the lattice separation, while one estimates the ultraviolet cutoff Λ to be of the order of $1/x_0$, yielding $\Lambda/\rho_0 \approx 2$. The open and closed symbols in Fig. 2.4 show the exact diagonalization results for $S_2(n=1) - \ln(N)$ as a function of g for $N = 13$. The three lines correspond to the prediction from the TLL theory for slightly

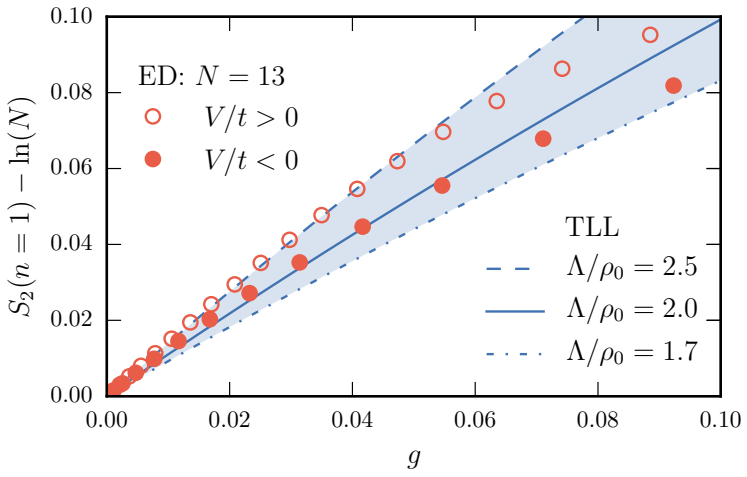

Figure 2.4: The effective interaction dependence of the 1-particle partition second Rényi entanglement entropy $S_2(n=1) - \ln(N)$. Open (closed) points were computed via exact diagonalization of the $t-V$ model for $N = 13$ with repulsive (attractive) interactions. The lines show the prediction from the Tomonaga-Luttinger liquid theory for three different values of the ultraviolet cutoff Λ measured in units of the density ρ_0.

different values of the UV cutoff Λ. Due to the highly non-linear relationship between the interaction strength V/t and the TLL parameter K (Eq. 2.19), in combination with the sensitivity of the particle partition entanglement to the strength and nature of inter-particle interactions, it is no surprise that the EE in the $t-V$ model is a multi-valued function of the effective interaction parameter g for attractive and repulsive interactions. Clearly, high energy lattice-scale physics, not captured within the low energy TLL theory is responsible for this behavior. Moreover, recall that the ultraviolet cutoff, Λ, in Eq. (2.5), is proportional to the inverse of the effective range of the interaction [42]. Therefore, we expect Λ to exhibit a dependence on the nature and strength of the interaction,

i.e., have K-dependence [29]. Considering such a dependence, we find that the $t-V$ model results for $S_2(n=1)-\ln(N)$ are bounded by the theoretically calculated ones using $\Lambda/\rho_0 = 1.7$ and 2.5 (Fig. 2.4). Note that both ratios are of order 2.

Testing the proposed leading order scaling of the particle partition EE in Eq. (2.4) with the partition size n in the TLL phase, requires the calculation of n-RDM with $n > 1$. While this can be done in principle using standard techniques [41], the resulting evaluation of $S_2(n)$ requires performing $2n$ non-separable integrals. Even for the $n = 2$ we were not able to analytically extract the asymptotic scaling of Tr ρ_2^2. However, from numerical exact diagonalization of the $t-V$ model in the in the TLL phase we were able to calculate the Rényi EEs for partitions up to $n = N/2 = 5$ for $N = 10$ as seen in Fig. 2.5. Our results are in agreement with previous calculations of $N = 6, n = 3$ [24]

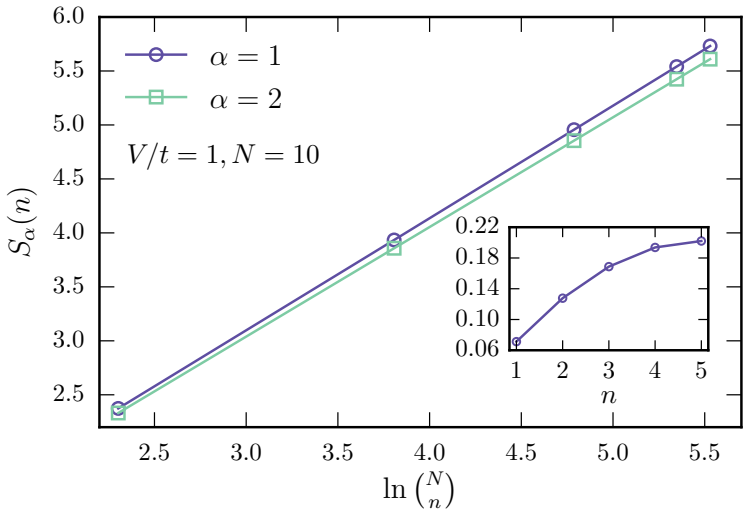

Figure 2.5: Scaling of $S_\alpha(n)$ with $\ln \binom{N}{n}$ for $\alpha = 1, 2$ in the ground state of the $t-V$ model with $V/t = 1$, $N = 10$, and for partition sizes $1 \leq n \leq 5$. Inset: Interaction contribution to the EE $(S_1(n) - \ln \binom{N}{n})$ vs n.

and strongly suggest that the leading term in the scaling of the Rényi EEs with n is indeed equal to the Rényi EE of free fermions, i.e., $\ln \binom{N}{n}$. Interactions introduce a correction term that increases with the partition size with a negative curvature (see Fig. 2.5 inset) such that both the leading order constant and

finite-size power-law corrections to scaling both depend on n.

Finally we investigate the question of whether particle bipartition EE is sensitive to the ground state degeneracy known to occur in the $t-V$ model with periodic boundary conditions and an even number of sites. Introducing the inversion operator P [47] defined by

$$Pc_i^\dagger P^\dagger = c_{M-i+1}^\dagger, \quad i = 1, \cdots, M. \tag{2.22}$$

where P commutes with the Hamiltonian of the $t-V$ model in Eq. (2.18) for PBC, we can write the degenerate ground state as a superposition of the eigenstates of the inversion operator: $P|\Phi_\pm\rangle = \pm|\Phi_\pm\rangle$, i.e.,

$$|\Psi\rangle = \cos(\theta)|\Phi_+\rangle + \sin(\theta)|\Phi_-\rangle. \tag{2.23}$$

Here, we only consider a superposition with real coefficients that can be varied through the parameter $0 \leq \theta \leq \pi$ and study the dependence of the Rényi EEs on θ as seen in Fig. 2.6. Our numerical results for repulsive interactions with $N = 10$ show that $S_1(n = 1)$ oscillates with θ (Fig. 2.6 inset), where the maximum EE corresponds to $|\Psi\rangle$ being an eigenstate of P, i.e., $\theta = 0$ or $\theta = \pi/2$, and the minimum EE is obtained when both eigenstates $|\Phi_\pm\rangle$ contribute equally to $|\Psi\rangle$ (maximum uncertainty in P, $\theta = \pi/4, 3\pi/4$). Moreover, the difference between the lower and upper bound vanishes in the non-interacting limit and widens with increasing interaction strength up to $\ln 2$ in the limit $V/t \to \infty$ (see Appendix C). Interestingly, Fig. 2.6 shows that for $\theta = \pi/4$, $S_1(n = 1)$ exhibits a peak near the critical point ($V/t = 2$), while the $S_1(n = 1)$ dependence on V/t for $\theta = 0$ is very similar to that obtained from the non-degenerate ground state using APBC.

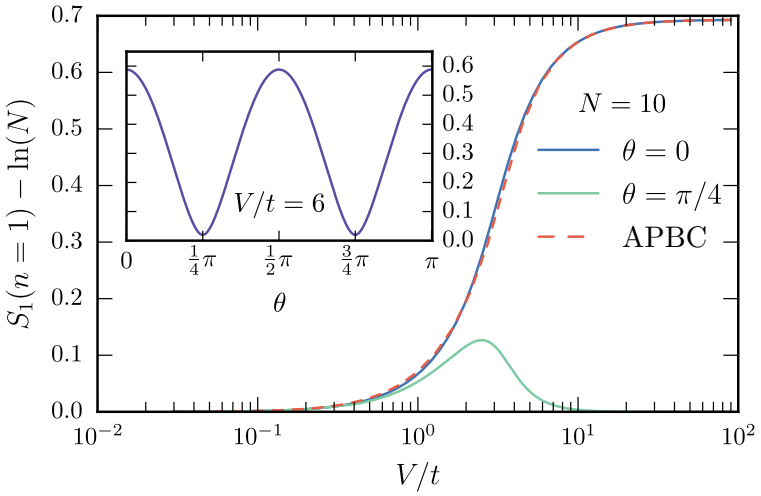

Figure 2.6: Effects of ground state degeneracy. The $S_2(n = 1) - \ln(N)$ dependence on V/t in the ground state of the $t - V$ model for $N = 10$. Solid lines represent results obtained from the degenerate ground state in Eq. (2.23) using PBC and $\theta = 0, \pi/4$ (see the text for details). The dashed line corresponds to the non-degenerate ground state for APBC. Inset: $S_2(n = 1) - \ln(N)$ vs θ for $V/t = 6$.

2.6 Conclusions

In this paper we have studied the finite size and interaction dependence of the particle partition Rényi entanglement entropies of a fermionic Tomonaga-Luttinger liquid and find that:

$$S_\alpha(n, N) = \ln \binom{N}{n} + a_\alpha(n) + \mathcal{O}\left(\frac{1}{N^{\gamma_\alpha(n)}}\right) \tag{2.24}$$

where n is the number of particles in the subsystem and α the Rényi index. This result is in agreement with the empirical prediction made in Ref. [22]. For the special case $n = 1,\ \alpha = 2$ we have determined the power of the finite size correction to the leading logarithm to be $\gamma_2(1) = K + K^{-1} - 1$ where K is the Luttinger parameter and confirmed this interaction dependence for the $t - V$ model by mapping it to the exactly solvable XXZ chain. The more general result for $n > 1,\ \alpha \neq 2$ in Eq. (2.24) is supported by extensive exact diagonalization results on the lattice $t - V$ model of spinless fermions obtained

on systems with up to $M = 28$ sites. This general scaling form can be contrasted with a bosonic Tomonaga-Luttinger liquid, where it was found [29] that $S_2(n, N) \simeq (n/K) \ln N + a_2'(n) + \mathcal{O}(1/N^{1-K^{-1}})$ which asymptotically recovers the free fermion result in the limit of hard-core bosons ($K \to 1^+$) using the fact that $\binom{N}{n} \approx N^n/n!$ for $N \gg n$.

The universality of the prefactor of the leading order logarithm in Eq. (2.24) demonstrates that due to the required anti-symmetrization of the N-particle wavefunction, fermions are always more entangled than bosons under a particle partition. This is consistent with what was numerically found for hard-core particles with variable anyonic statistics [27]. Such sensitivity to particle statistics and interaction dependence is absent in the asymptotic scaling of the spatial mode entanglement entropy for critical $(1 + 1)$-dimensional systems where the prefactor is universal and related to the central charge of the underlying conformal field theory [31]. Thus, the particle partition entanglement appears to be a useful diagnostic of quantum correlations in many-body systems, and its logarithmic scaling with the total number of particles N highlights the potential utility of protocols [21] that aim to transfer it to experimentally accessible mode entanglement.

An interesting open question remains on the origin and development with system size of the peak in the entanglement entropy in the ground state of the $t - V$ model near the continuous phase transition at $V/t = 2$ for macroscopic particle partitions with $n = N/2$ (Fig. 2.2 (b)). A careful finite-size analysis of this unexpected feature (due to the lack of any natural length scale describing the partition) would require moving beyond exact diagonalization and employing recently adapted hybrid Monte Carlo methods [39, 48, 49].

Chapter 3

Operationally Accessible Entanglement Entropy in the tV Model

3.1 Operationally Accessible Entanglement Entropy

The quantum entanglement present between the constituents of a system can be quantified via von Neumann and Rényi entanglement entropies. These measures have been shown to be sensitive to phase transitions in physical models, which is one of the reasons for the study of quantum entanglement. But, what about using entanglement as a resource for, let's say, quantum computing? For this purpose, the entanglement entropies have to be redefined such that they obey constraints imposed by performing a measurement on a system. These physical constraints imposed on the quantum systems that can be prepared are known as superselection rules (SSR) and can be based off particle number or spin conservation, for example. The amount of entanglement that is actually accessible as a resource is then subject to these SSR's.

In this chapter, the accessible entanglement entropy is presented. In the first section, a review of the von Neumann and Rényi entanglement entropies is given. In the second, analytical values for the spatial entanglement entropies are derived at various regimes of the $t - V$ model. Finally, numerical results obtained via exact diagonalization are presented.

3.1.1 The Rényi Entanglement Entropy

The amount of entanglement that exists between some partition A and its compliment B of a quantum many-body system in pure state $|\Psi\rangle$ can be quantified via the Rényi entanglement entropy which depends on an index α:

$$S_\alpha(\rho_A) = \frac{1}{1-\alpha} \ln \mathrm{Tr}\ \rho_A^\alpha \tag{3.1}$$

where ρ_A is the reduced density matrix of partition A obtained by tracing out all degrees of freedom in B from the full density matrix:

$$\rho_A = \mathrm{Tr}_B\ \rho = \mathrm{Tr}_B\, |\Psi\rangle \langle\Psi| \ . \tag{3.2}$$

The Rényi entropy is a monotonically decreasing function of α for $\alpha > 1$ and is bounded from above by the von Neumann entropy, $S_1(\rho_A) = -\,\mathrm{Tr}\, \rho_A \ln \rho_A$.

For a quantum many-body system subject to physical laws conserving some quantity (particle number, charge, spin, etc.), the set of local operations on the state $|\Psi\rangle$ are limited to those that don't violate the corresponding global superselection rule. For the remainder of this paper, we will focus on our discussion on the case of fixed total N and thus we are restricted to only those operators which locally preserve the particle number in A. The effect this has on the amount of entanglement that can be transferred to a qubit register is apparent from the simple example (adapted from Ref. [11] of one particle confined to two spatial modes A and B corresponding to site occupations.

Then, for the state $|\Psi\rangle = (|1\rangle_A \otimes |0\rangle_B + |0\rangle_A \otimes |1\rangle_B)/\sqrt{2}$, Eq. (3.1) gives that $S_1 = \ln 2$. However, this entanglement cannot be transferred to a register prepared in initial state $|0\rangle_R$ via a SWAP gate. In quantum circuits, a SWAP in Hilbert Space A, will take the state of the A subregion of a resource, and swap it with the state of the A subregion of a register. Let $|\Psi\rangle$ be the resource state and $|0\rangle_R$ the register, then acting with a SWAP gate gives:

$$\begin{aligned}&\texttt{SWAP}\,|0\rangle_R \otimes (|1\rangle_A \otimes |0\rangle_B + |0\rangle_A \otimes |1\rangle_B)/\sqrt{2}\\ &= \frac{1}{\sqrt{2}}(|0\rangle_R \otimes |0\rangle_A \otimes |1\rangle_B + |1\rangle_R \otimes |0\rangle_A \otimes |0\rangle_B)\end{aligned}$$

The last term is not physically allowed due to the restriction that the number of particles in the system is fixed to be 1. The post-swap result remains in a product state and the amount of transferable entanglement is identically zero. The SWAP gate in the example above takes the register modes and exchanges them with the modes in subsystem A of the resource:

$$\texttt{SWAP}\,|\phi\rangle_R \otimes |\psi\rangle_A = |\psi\rangle_R \otimes |\phi\rangle_A \tag{3.3}$$

The SWAP can be defined such that it exchanges resource modes with modes in B instead. Formally, this gate is a product of three controlled-not (CNOT) gates:

$$\texttt{SWAP}\,|\phi\rangle_R \otimes |\psi\rangle_A = \texttt{CNOT}_{R,A}\texttt{CNOT}_{A,R}\texttt{CNOT}_{R,A}\,|\phi\rangle_R \otimes |\psi\rangle_A \tag{3.4}$$

where the subscript left to the comma denotes the control mode and the one to the right of the comma, the target. The CNOT acts on qubit modes. That is, each of the modes will be either one of two values, call them 1 and 0. If the control qubit is equal to 1, then the value of the target is 'flipped' to the other possible value. If the control qubit is 0, the target is left unchanged.

3.1.2 von Neumann Accessible Entanglement: $\alpha = 1$

Thus, Eq. (3.1), which includes the effects of non-local number fluctuations between A and B, overcounts the amount of entanglement that can be accessed from the system. To quantify the physical reduction, Wiseman and Vaccaro [3] suggested that for the case of $\alpha = 1$ a more appropriate measure should weight contributions to the entanglement coming from each superselection sector corresponding to the number of particles n in A:

$$S_1^{\rm acc}(\rho_A) = \sum_{n=0}^{N} P_n S_1(\rho_{A_n}). \tag{3.5}$$

Here ρ_{A_n} is defined to be the reduced density matrix of A, projected onto the subspace of fixed local particle number n

$$\rho_{A_n} = \frac{1}{P_n} \mathcal{P}_{A_n} \rho_A \mathcal{P}_{A_n} \tag{3.6}$$

accomplished via a projection operator $\mathcal{P}_{A_n}$ where $\mathcal{P}_{A_n} |\Psi\rangle = |n\rangle_A \otimes |N-n\rangle_B$. P_n is the probability of measuring n particles in A:

$$P_n = \mathrm{Tr}\, \mathcal{P}_{A_n} \rho_A \mathcal{P}_{A_n} = \langle \Psi | \mathcal{P}_{A_n} | \Psi \rangle . \tag{3.7}$$

As the projection constitutes a local operation which can only decrease entanglement, it is clear that $S_1^{\rm acc}(\rho_A) \leq S_1(\rho_A)$. Moreover, the difference

$$\Delta S_1(\rho_A) \equiv S_1(\rho_A) - S_1^{\rm acc}(\rho_A) \tag{3.8}$$

can be determined by noting that the superselection rule guarantees that $[\rho_A, \hat{n}] = 0$ where $\hat{n}$ is the number operator acting in partition A. Thus ρ_A is block-diagonal in n and it can be shown [50] that

$$\Delta S_1(\rho_A) = H_1(\{P_n\}) \tag{3.9}$$

where

$$H_1(\{P_n\}) = -\sum_{n=0}^{N} P_n \ln P_n. \tag{3.10}$$

is the Shannon entropy of the number probability distribution. It is instructive to consider Eq. (3.9) for the special case of a discrete Gaussian distribution, $P_n \propto e^{-(n-\langle n\rangle)^2/2\sigma^2}$ where $H_1 = \ln\left(2\pi e\sigma^2 + \frac{1}{12}\right)$ depends only on the variance of P_n

$$\sigma^2 \equiv \left\langle n^2 \right\rangle - \langle n \rangle^2 = \sum_{n=0}^{N} n^2 P_n - \left(\sum_{n=0}^{N} n P_n\right)^2. \tag{3.11}$$

Thus, when the number fluctuations are Gaussian, the von Neumann accessible entanglement is completely determined by the variance.

3.1.3 Rényi Accessible Entanglement: $\alpha \neq 1$

Computing the accessible entanglement for a many-body system is a difficult task for $\alpha = 1$, as full state tomography is required to reconstruct the density matrix ρ. However, for integer values with $\alpha > 1$ a replica trick can be used to recast $\mathrm{Tr}\rho_A^\alpha$ as the expectation value of some local operator [31]. This advance has led to a boon of new entanglement results using both computational [1, 38, 39, 51, 52] and experimental [2, 53–57] methods. Motivated by this progress, [4] generalized the accessible entanglement to the case of Rényi entropies with $\alpha \neq 1$ and found that:

$$S_\alpha^{\mathrm{acc}}(\rho_A) = \frac{\alpha}{1-\alpha} \ln\left[\sum_n P_n \mathrm{e}^{\frac{1-\alpha}{\alpha} S_\alpha(\rho_{A_n})}\right] \tag{3.12}$$

which reproduces Eq. (3.5) in the limit $\alpha \to 1$. While not physically transparent in this form, the modification from the $\alpha = 1$ case results from replacing the geometric mean in Eq. (3.5) with a general power mean whose form is constrained by the physical requirement that

$$0 \leq \Delta S_\alpha \leq \ln(N+1) \tag{3.13}$$

where the upper bound is equal to the support of P_n. Eq. (3.71) can also be interpreted as the quantum generalization of the conditional classical Rényi entropy [58–62], subject to physical constraints [4]. The arguments leading to Eq. (3.9) can then be generalized (see the supplemental material of Ref. [[4]]) leading to

$$\Delta S_\alpha \equiv S_\alpha - S_\alpha^{\text{acc}} = H_{1/\alpha}\left(\{P_{n,\alpha}\}\right) \tag{3.14}$$

where we introduce the classical Rényi entropy of P_n

$$H_\alpha\left(\{P_n\}\right) = \frac{1}{1-\alpha} \ln \sum_n P_n^\alpha \tag{3.15}$$

and

$$P_{n,\alpha} = \frac{\text{Tr}\ [\mathcal{P}_{A_n} \rho_A^\alpha \mathcal{P}_{A_n}]}{\text{Tr}\ \rho_A^\alpha} = \frac{P_n^\alpha\ \text{Tr}\ \rho_{A_n}^\alpha}{\text{Tr}\ \rho_A^\alpha} \tag{3.16}$$

can be interpreted as a normalization of partial traces of ρ_A^α, where the SSR fixing the total particle number leads to $\text{Tr}\ \rho_A^\alpha = \sum_n \text{Tr}\ [\mathcal{P}_{A_n} \rho_A^\alpha \mathcal{P}_{A_n}]$ and thus guarantees the normalization of $P_{n,\alpha}$. Note that we have defined $P_{n,1} \equiv P_n$ for notational consistency. For brevity, let $H_\alpha(\{P_n\}) \equiv H_\alpha$ from here onwards.

Writing the difference ΔS_α as the classical Rényi entropy of the fictitious probability distribution $P_{n,\alpha}$, simplifies the calculation of ΔS_α and clarifies its properties, e.g., the fact that H_α is positive and bounded from above by $H_0 = \ln(N+1)$ guarantees that ΔS_α satisfies the physical requirement in Eq. (3.13). In addition, $P_{n,\alpha}$ is fully determined by P_n and the full and the projected traces of ρ_A^α, i.e. $\text{Tr}\ \rho_A^\alpha$ and $\text{Tr}\ \rho_{A_n}^\alpha$, which can be measured using the experimental and numerical methods mentioned above.

3.1.4 Projecting onto subspaces of fixed local particle number

Knowing the density matrix of subregion A will suffice to calculate spatial Entanglement Entropy. Nevertheless, to get the accessible entanglement, simply

knowing ρ_A is not enough. The reduced density matrix of A, projected onto the subspace of fixed local particle number n is needed. To recap, the spatial Rényi Entanglement Entropy is given by:

$$S_\alpha(\rho_A) = \frac{1}{1-\alpha} \ln \mathrm{Tr}\{\rho_A^\alpha\} \tag{3.17}$$

Where α is the Rényi Index and ρ_A is the density matrix of subregion A. This calculation is still required to get accessible entanglement but, as shall be seen, a few extra steps have to be taken to make sure that local particle number conservation is being satisfied. The first of these extra steps will be to project ρ_A to subspaces of local particle number. Projection operators can be written as diagonal matrices with ones on the entries corresponding to the subspace for which the projection is desired and zeros for the rest. Knowing this, the projection operators onto subspaces of fixed local particle numbers can be built rather simply. The projected reduced density matrix of A into the subspace of fixed local particle number n is obtained by:

$$\rho_{A_n} = \frac{1}{P_n} \mathcal{P}_{A_n} \rho_A \mathcal{P}_{A_n} \tag{3.18}$$

Where P_n is the probability of measuring an A state with n particles and $\mathcal{P}_{A_n}$ is the projection operator onto the subspace of local particle number n.

After all this preamble, the accessible entanglement can now be obtained. The accessible entanglement is:

$$S_\alpha^{\mathrm{acc}}(\rho_A) = \sum_n P_n S(\rho_{A_n}) \tag{3.19}$$

Where the sum is carried over all possible local particle numbers that Alice may have. In other words, $n = 0, 1, ..., N - n_B$.

In the next section, analytical $S_\alpha^{\mathrm{acc}}(\rho_A)$ values will be derived in various regimes of the $t - V$ Model.

3.2 Analytical predictions in the $t-V$ Model

The $t-V$ Model describes N itinerant spinless fermions on a one dimensional lattice consisting of L sites under periodic boundary conditions:

$$H = -t\sum_i \left(c_i^\dagger c_{i+1} + c_{i+1}^\dagger c_i\right) + V\sum_i n_i n_{i+1} \tag{3.20}$$

where $c_i^\dagger(c_i)$ creates(annihilates) a fermion on site i, n_i counts the number of fermions on site i and t, V are tunable parameters that characterize the tunneling or hopping rate and the interaction strength, respectively. The first sum is carried over all pairs of neighboring lattice sites. It is customary to make $\mathcal{H}$ dimensionless by dividing t throughout and thus having the interaction strength V/t be the only tunable parameter.

There are three phases that occur in the $t-V$ Model. The Phase Separated Solid (PSS) occurs at $V/t \ll -2$. Here, the attractive interaction leads to fermions clustering into large groups of particles that occupy adjacent lattice sites. On the contrary, at $V/t \gg 2$, the repulsive interaction leads to fermions trying to get as far as possible from each other, forming an alternating pattern of fermion-vacancy-fermion-vacancy and so on and so forth. This phase is known as a Charged Density Wave (CDW). The remaining phase in this model is the Tomonaga Luttinger-Liquid (TLL), which occurs for $-2 < V/t < 2$. Here, the fermions could be in any possible configuration but the probability amplitudes for each of these will depend on the value of the interaction strength. The PSS-TLL transition is a first order transition while the TLL-CDW transition is continuous.

In this section, analytical values for the operationally accessible von Neumann entropy, $S_1^{\text{acc}}(\rho_A)$, will be derived in all phases of the $t-V$ Model and also at the first order phase transition. Then, the results for the Rényi accessible entanglement entropies, $S_\alpha^{\text{acc}}(\rho_A)$, will be shown. Derivations will not be

done in detail for $S_\alpha^{\text{acc}}(\rho_A)$ since the calculation steps are essentially identical to those of $S_1^{\text{acc}}(\rho_A)$.

3.2.1 Infinitely repulsive interaction

The state in this limit is known as a charged density wave (CDW). An infinitely strong repulsion between the particles in the system, makes them want to be as far away from each other as possible. This results in the particles forming an alternating pattern of filled-vacant-filled-vacant ... lattice sites. Thus, there are 2 possible configurations: one, that goes as filled-vacant-filled ... and another that goes as $vacant - filled - vacant$ .... Thus, in the occupation number basis, the CDW state is:

$$|\Psi\rangle_{CDW} = \frac{1}{\sqrt{2}}[|101010...\rangle + |010101...\rangle] \tag{3.21}$$

Where 1 denotes that the site is occupied and 0, that it is vacant. The coefficient before the bracket is a normalization constant. As will be shown, the accessible entanglement for this state is dependent on the parity of the total number of particles N. Up next, the result for even N will be derived.

3.2.1.1 Even N

In the following calculations, the system will be partitioned into spatial subregions A and B, both containing the same number of sites. In other words, if the total number of sites in the $t-V$ chain is L, then the partition size will be $l = \frac{L}{2}$.

In the case of even particle number N, the CDW state will have the same number of particles in each subregion A and B:

$$|\Psi\rangle_{N_{Even}} = \frac{1}{\sqrt{2}}[|\underbrace{1010...}_{\frac{N}{2}particles}, \underbrace{1010...}_{\frac{N}{2}particles}\rangle + |\underbrace{0101...}_{\frac{N}{2}particles}, \underbrace{0101...}_{\frac{N}{2}particles}\rangle] \tag{3.22}$$

As a reminder, labels left to the comma correspond to spatial subregion A, while those to the right correspond to B.

The full density matrix ρ_{AB} takes the form:

$$\begin{aligned}\rho_{AB} &= |\Psi\rangle_{N_{Even}}\langle\Psi|_{N_{Even}} \\ &= \frac{1}{2}|0101..., 0101\rangle\langle 0101..., 0101...| + \frac{1}{2}|0101..., 0101\rangle\langle 1010..., 1010...| \\ &+ \frac{1}{2}|1010..., 1010\rangle\langle 0101..., 0101...| + \frac{1}{2}|1010..., 1010\rangle\langle 1010..., 1010...|\end{aligned} \tag{3.23}$$

Recall that to calculate the entanglement entropies, it is necessary to obtain the reduced density matrix of subsystem A. Taking the partial trace with respect to B, the reduced density matrix of A is obtained:

$$\rho_A = \mathrm{Tr}_B\, \rho_{AB} \quad = \sum_n {}_B\langle n|\Psi\rangle\langle\Psi|n\rangle_B \tag{3.24}$$

The summation above is carried over all possible states that B can be found in. In this case, there are only two possible B states: $n = |0101...\rangle_B$ and $n = |1010...\rangle_B$. Thus, taking the partial trace respect to B, the reduced density matrix of A becomes:

$$\rho_A = \frac{1}{2}(|0101...\rangle_A\langle 0101...|_A + |1010...\rangle_A\langle 1010...|_A) \tag{3.25}$$

Notice that some of the terms have vanished due to the orthonormality of the states. At this point, it will be convenient for purposes of illustration to rewrite the reduced density matrix of A in actual matrix form rather than in Dirac or Bra-Ket notation. Following the convention $|0101\ldots\rangle_A$ and $|1010\ldots\rangle_A$ for columns and rows from left to right and top to bottom, respectively, the reduced density matrix of A can be written as:

$$\rho_A = \begin{pmatrix} \frac{1}{2} & 0 \\ 0 & \frac{1}{2} \end{pmatrix} \tag{3.26}$$

For spatial entanglement, ρ_A would suffice, but for accessible entanglement, the matrix has to now be projected onto the various subspaces or sectors of fixed local particle number in A. In this case, both of the states share the same local particle number. That is, the states: $|1010...\rangle_A$ and $|0101...\rangle_A$ both have local particle number $n = \frac{N}{2}$. Since ρ_A only contains entries corresponding to states with the same particle number, no projection is needed. In other words, for this state $\rho_A = \rho_{A_{\frac{N}{2}}}$. Taking the partial trace of $\rho_A = \rho_{A_{\frac{N}{2}}}$, the probability of measuring a state with local particle number $n = \frac{N}{2}$ is unity, $P_{\frac{N}{2}} = 1$. The projected and normalized reduced density matrix of A is now known and can be substituted into 3.19 to calculate the accessible entanglement entropy:

$$\begin{aligned} S_1^{\text{acc}}(\rho_A) &= \sum_n P_n S_1(\rho_{A_n}) \\ &= -P_{\frac{N}{2}} \operatorname{Tr}\left\{\rho_{A_{\frac{N}{2}}} \ln \rho_{A_{\frac{N}{2}}}\right\} \\ &= -\operatorname{Tr}\left\{ \begin{pmatrix} \frac{1}{2} & 0 \\ 0 & \frac{1}{2} \end{pmatrix} \begin{pmatrix} \ln \frac{1}{2} & 0 \\ 0 & \ln \frac{1}{2} \end{pmatrix} \right\} \qquad (3.27) \\ &= -\ln \frac{1}{2} \qquad (3.28) \\ S_1^{\text{acc}}(\rho_A) &= \ln 2 \qquad (3.29) \end{aligned}$$

Thus, for even N and $V/t \to +\infty$, the accessible entanglement converges to $\ln 2 \approx 0.6931\ldots$. Up next, the result for odd N will be derived.

3.2.1.2 Odd N

The most general state is:

$$|\Psi\rangle_{N_{Odd}} = \frac{1}{\sqrt{2}}[|\underbrace{...101}_{\frac{N+1}{2}particles}, \underbrace{010...}_{\frac{N-1}{2}particles}\rangle + |\underbrace{...010}_{\frac{N-1}{2}particles}, \underbrace{101...}_{\frac{N+1}{2}particles}\rangle] \qquad (3.30)$$

Note that now when doing an equal spatial bipartition, one of the subregions will have one more particle than the other, unlike the even particle case in

which both subregions had the same number of particles. Specifically, one of the subregions will have $\frac{N+1}{2}$ and the other, $\frac{N-1}{2}$. This implies that ρ_A will have to be projected onto the space of local particle number $\frac{N+1}{2}$ and then onto $\frac{N-1}{2}$. But before doing that, again the full body density matrix is needed:

$$\begin{aligned}\rho_{AB} &= |\Psi\rangle_{N_{Odd}}\langle\Psi|_{N_{Odd}} \\ &= \frac{1}{2}(|...101,010...\rangle\langle...101,010...| + |...101,010...\rangle\langle...010,101...| \\ &+ |...010,101...\rangle\langle...101,010...| + |...010,101...\rangle\langle...010,101...|)\end{aligned} \tag{3.31}$$

The possible B states are: $n = |101...\rangle, |010...\rangle$ with $\frac{N+1}{2}$ and $\frac{N-1}{2}$ particles, respectively. Taking the partial trace respect to B, the reduced density matrix of A becomes:

$$\rho_A = \frac{1}{2}(|101...\rangle_A\langle 101...|_A + |010...\rangle_A\langle 010...|_A) \tag{3.32}$$

Once again, it may be more illustrative to rewrite in matrix form. Defining an orthonormal basis $|101...\rangle_A = \begin{pmatrix} 1 \\ 0 \end{pmatrix}$ and $|010...\rangle_A = \begin{pmatrix} 0 \\ 1 \end{pmatrix}$ the reduced density matrix of A becomes:

$$\rho_A = \begin{pmatrix} \frac{1}{2} & 0 \\ 0 & \frac{1}{2} \end{pmatrix} \tag{3.33}$$

The simple projection operators onto $\frac{N+1}{2}$ and $\frac{N-1}{2}$ particle space in this basis are:

$$\mathcal{P}_{A_{\frac{N+1}{2}}} = \begin{pmatrix} 1 & 0 \\ 0 & 0 \end{pmatrix}, \mathcal{P}_{\frac{N-1}{2}} = \begin{pmatrix} 0 & 0 \\ 0 & 1 \end{pmatrix} \tag{3.34}$$

Applying these projections to ρ_A and choosing the probability such that the trace of each matrix is unity (normalization), the projected reduced density

matrices become:

$$\rho_{A_{\frac{N+1}{2}}} = \begin{pmatrix} 1 & 0 \\ 0 & 0 \end{pmatrix} \text{ with probability } P_{\frac{N+1}{2}} = \frac{1}{2} \tag{3.35}$$

and

$$\rho_{A_{\frac{N-1}{2}}} = \begin{pmatrix} 0 & 0 \\ 0 & 1 \end{pmatrix} \text{ with probability } P_{\frac{N-1}{2}} = \frac{1}{2} \tag{3.36}$$

Substituting into the accessible entanglement equation (3.19):

$$\begin{aligned} S_1^{\text{acc}}(\rho_A) &= \sum_n P_n S_\alpha(\rho_{A_n}) \\ &= -(\frac{1}{2}) \operatorname{Tr}\left\{ \begin{pmatrix} 1 & 0 \\ 0 & 0 \end{pmatrix} \ln \begin{pmatrix} 1 & 0 \\ 0 & 0 \end{pmatrix} \right\} - (\frac{1}{2}) \operatorname{Tr}\left\{ \begin{pmatrix} 1 & 0 \\ 0 & 0 \end{pmatrix} \ln \begin{pmatrix} 1 & 0 \\ 0 & 0 \end{pmatrix} \right\} \\ S_1^{\text{acc}}(\rho_A) &= 0 \end{aligned} \tag{3.37}$$

because $\ln 1 = 0$ and thus the traces in both terms vanish. Therefore, the accessible entanglement vanishes in the infinite repulsion limit ($V/t \to +\infty$) with odd number of total particles in the system.

The results for the accessible entanglement in the infinitely repulsive limit can then be summarized as:

$$\lim_{V \to +\infty} S_1^{acc} = \begin{cases} \ln 2 & \text{if } N \text{ is even} \\ 0 & \text{if } N \text{ is odd} \end{cases} \tag{3.38}$$

3.2.2 Infinitely attractive interaction

In this section, an analytical result will be derived at half-filling ($L = 2N$) and partition size equal to half the number of sites ($\ell = \frac{L}{2}$) for $V/t \to -\infty$. After arriving to the half-filling result, a general result, for any filling fraction and partition size, will be also derived.

3.2.2.1 Half-filling

In the $V/t \to -\infty$ regime of the $t-V$ model, the fermions experience an infinitely strong attraction to each other. As a consequence, they cluster together into groups of particles all in neighboring sites to each other. The total possible number of such cluster configurations is equal to the number of sites L. Thus, the most general state in this regime is:

$$|\Psi\rangle_{PSS} = \frac{1}{\sqrt{L}}[|\underbrace{111...111}_{Nparticles},\underbrace{000...000}_{Nvacancies}\rangle + |011...111, 100...000\rangle + |001...111, 110...000\rangle$$
$$+... + |\underbrace{000...000}_{Nvacancies},\underbrace{111...111}_{Nparticles}\rangle + |100...000, 011...111\rangle + ...|111...110, 000...001\rangle] \tag{3.39}$$

This state is known as a phase separated solid (PSS). Since there are a total of L possible configurations, hence the normalization constant $\frac{1}{\sqrt{L}}$.

In an effort to simplify the notation while keeping the calculation general, the A or B states will be relabeled as:

$$|111...111\rangle_A \to |N\rangle$$
$$|011...111\rangle_A \to |N-1\rangle$$
$$|001...111\rangle_A \to |N-2\rangle$$
$$\vdots$$
$$|000...011\rangle_A \to |2\rangle$$
$$|000...001\rangle_A \to |1\rangle$$
$$|000...000\rangle_A \to |0\rangle$$

There is still one flaw with this notation. A $|N-1\rangle$ state could represent either $|011...111\rangle$ or $|111...110\rangle$. In other words, even though they have the same local particle number $N-1$, the configurations themselves are different.

One way in which this problem can be circumvented is by adding a subscript to the label to represent distinct configurations. Since particle number will only be shared between two distinct particle configurations, using subscripts of 1 and 2 seems natural. For example: $|011...111\rangle \rightarrow |(N-1)_1\rangle$ and $|111...110\rangle \rightarrow |(N-1)_2\rangle$. $|\Psi\rangle_{PSS}$ now becomes:

$$|\Psi\rangle_{PSS} = \frac{1}{\sqrt{L}}[|N,0\rangle + |(N-1)_1, 1_1\rangle + |(N-2)_1, 2_1\rangle + ... + |0,N\rangle + |1_2, (N-1)_2\rangle + ... |(N-1)_2, 1_2\rangle] \tag{3.40}$$

Taking the outer product of Eq. (3.40) with itself, the full body density matrix is obtained:

$$\rho_{AB} = |\Psi\rangle_{PSS}\langle\Psi|_{PSS} = \begin{pmatrix} \frac{1}{L} & \frac{1}{L} & ... & \frac{1}{L} \\ \frac{1}{L} & \frac{1}{L} & ... & \frac{1}{L} \\ \vdots & \vdots & \vdots & \vdots \\ \frac{1}{L} & \frac{1}{L} & ... & \frac{1}{L} \end{pmatrix} \tag{3.41}$$

The full body density matrix contains $L \times L$ with all entries equal to $\frac{1}{L}$. Before proceeding, the basis of this matrix should be described. Columns (from left to right) and rows (from top to bottom) are arranged as: $|N,0\rangle, |0,N\rangle, |(N-1)_1, 1_1\rangle, |(N-1)_2, 1_2\rangle, |(N-2)_1, 2_1\rangle, |(N-2)_2, 2_2\rangle, ..., |2_1, (N-2)_1\rangle, \rangle, |2_2, (N-2)_2\rangle, \rangle, |1_1, (N-1)_1\rangle, \rangle, |1_2, (N-1)_2\rangle$. Notice that configurations that share local particle number have been paired up next to each other in the prescribed ordering scheme. The first two states are exceptions, as their subregions never share the same local particle number with subregions of any other state. Now that the basis has been explained, it's time to get the reduced density matrix of A.

Taking the partial trace with respect to B of Eq. (3.41), the reduced density

matrix becomes:

$$\rho_A = \begin{pmatrix} \frac{1}{L} & 0 & ... & 0 & 0 \\ 0 & \frac{1}{L} & ... & 0 & 0 \\ \vdots & \vdots & \ddots & \vdots & \vdots \\ 0 & 0 & ... & \frac{1}{L} & 0 \\ 0 & 0 & ... & 0 & \frac{1}{L} \end{pmatrix} \tag{3.42}$$

In the above matrix, the rows and columns correspond to the following configurations and in the following order: $|N\rangle_A, |0\rangle_A, |(N-1)_1\rangle_A, |(N-1)_2\rangle_A, |(N-2)_1\rangle_A, |(N-2)_2\rangle_A, ..., |2_1\rangle_A, |2_2\rangle_A, |1_1\rangle_A, |1_2\rangle_A$.

Now, ρ_A has to be projected onto the subspaces of local particle numbers. The allowed local particle numbers are: $n = N, N-1, N-2....2, 1, 0$. So a total of $N+1$ projections need to be done. The projection operators for $n = 0$ and $n = N$ become:

$$\mathcal{P}_N = \begin{pmatrix} 1 & 0 & ... & 0 & 0 \\ 0 & 0 & ... & 0 & 0 \\ \vdots & \vdots & \ddots & \vdots & \vdots \\ 0 & 0 & ... & 0 & 0 \\ 0 & 0 & ... & 0 & 0 \end{pmatrix}, \mathcal{P}_0 = \begin{pmatrix} 0 & 0 & ... & 0 & 0 \\ 0 & 1 & ... & 0 & 0 \\ \vdots & \vdots & \ddots & \vdots & \vdots \\ 0 & 0 & ... & 0 & 0 \\ 0 & 0 & ... & 0 & 0 \end{pmatrix} \tag{3.43}$$

For the remaining $N-1$ states, there will be two consecutive non-zero entries in the diagonal corresponding to the different fixed local particle number pairs.

For example:

$$\mathcal{P}_{N-1} = \begin{pmatrix} 0 & & & & & & & & & 0 \\ & 0 & & & & & & & & \\ & & 1 & & & & & & & \\ & & & 1 & & & & & & \\ & & & & 0 & & & & & \\ & & & & & 0 & & & & \\ & & & & & & \ddots & & & \\ & & & & & & & 0 & & \\ 0 & & & & & & & & & 0 \end{pmatrix}$$

$$\mathcal{P}_{N-2} = \begin{pmatrix} 0 & & & & & & & & & 0 \\ & 0 & & & & & & & & \\ & & 0 & & & & & & & \\ & & & 0 & & & & & & \\ & & & & 1 & & & & & \\ & & & & & 1 & & & & \\ & & & & & & \ddots & & & \\ & & & & & & & 0 & & \\ 0 & & & & & & & & & 0 \end{pmatrix}, \mathcal{P}_1 = \begin{pmatrix} 0 & & & & & & & & & 0 \\ & 0 & & & & & & & & \\ & & 0 & & & & & & & \\ & & & 0 & & & & & & \\ & & & & 0 & & & & & \\ & & & & & 0 & & & & \\ & & & & & & \ddots & & & \\ & & & & & & & 1 & & \\ 0 & & & & & & & & & 1 \end{pmatrix} \tag{3.44}$$

Notice from the form of the projection operators that the projected reduced density matrices will be similar to each other but with the two non-zero entries shifted correspondingly in the diagonal. Thus, taking the projection onto $n = N - 1$ of ρ_A, the projected reduced density matrix of this particle sector

becomes:

$$\rho_{A_{N-1}} = \frac{1}{P_{N-1}} \hat{\mathcal{P}}_{N-1} \rho_A \hat{\mathcal{P}}_{N-1}$$

$$\rho_{A_{N-1}} = \frac{1}{P_{N-1}} \begin{pmatrix} 0 & & & & & & & & 0 \\ & 0 & & & & & & & \\ & & \frac{1}{L} & & & & & & \\ & & & \frac{1}{L} & & & & & \\ & & & & 0 & & & & \\ & & & & & 0 & & & \\ & & & & & & \ddots & & \\ & & & & & & & 0 & \\ 0 & & & & & & & & 0 \end{pmatrix} \tag{3.45}$$

The probability of measuring a state with local particle number $N-1$ can be obtained from normalization:

$$\mathrm{Tr}\{\rho_{A_{N-1}}\} = 1 \implies \frac{1}{P_{N-1}} \frac{2}{L} = 1 \implies P_{N-1} = \frac{2}{L} \tag{3.46}$$

Thus, the normalized projection onto $n = N-1$ of ρ_A is:

$$\rho_{A_{N-1}} = \begin{pmatrix} 0 & & & & & & & & 0 \\ & 0 & & & & & & & \\ & & \frac{1}{2} & & & & & & \\ & & & \frac{1}{2} & & & & & \\ & & & & 0 & & & & \\ & & & & & 0 & & & \\ & & & & & & \ddots & & \\ & & & & & & & 0 & \\ 0 & & & & & & & & 0 \end{pmatrix} \text{ ; with probability } P_{N-1} = \frac{2}{L} \tag{3.47}$$

For $n = N - 2$:

$$\rho_{A_{N-2}} = \begin{pmatrix} 0 & & & & & & & & 0 \\ & 0 & & & & & & & \\ & & 0 & & & & & & \\ & & & 0 & & & & & \\ & & & & \frac{1}{2} & & & & \\ & & & & & \frac{1}{2} & & & \\ & & & & & & \ddots & & \\ & & & & & & & 0 & \\ 0 & & & & & & & & 0 \end{pmatrix} \; ; \text{ with probability } P_{N-2} = \frac{2}{L} \quad (3.48)$$

and so on and so forth.

Similarly, ρ_{A_N} and ρ_{A_0} become:

$$\rho_{A_N} = \begin{pmatrix} 1 & & & & & & & & 0 \\ & 0 & & & & & & & \\ & & 0 & & & & & & \\ & & & 0 & & & & & \\ & & & & 0 & & & & \\ & & & & & 0 & & & \\ & & & & & & \ddots & & \\ & & & & & & & 0 & \\ 0 & & & & & & & & 0 \end{pmatrix}, \rho_{A_0} = \begin{pmatrix} 0 & & & & & & & & 0 \\ & 1 & & & & & & & \\ & & 0 & & & & & & \\ & & & 0 & & & & & \\ & & & & 0 & & & & \\ & & & & & 0 & & & \\ & & & & & & \ddots & & \\ & & & & & & & 0 & \\ 0 & & & & & & & & 0 \end{pmatrix} \quad (3.49)$$

with probabilities $P_N = P_0 = \frac{1}{L}$. Finally, the accessible entanglement becomes:

$$\begin{aligned}
S_1^{acc}(\rho_A) &= \sum_n P_n S_\alpha(\rho_{A_n}) \\
&= -[\frac{1}{L}\operatorname{Tr}\{\rho_{A_N}\ln\rho_{A_N}\} + \frac{1}{L}\operatorname{Tr}\{\rho_{A_0}\ln\rho_{A_0}\} + \frac{2}{L}\operatorname{Tr}\{\rho_{A_{N-1}}\ln\rho_{A_{N-1}}\} \\
&+ \frac{2}{L}\operatorname{Tr}\{\rho_{A_{N-2}}\ln\rho_{A_{N-2}}\} + \cdots + \frac{2}{L}\operatorname{Tr}\{\rho_{A_2}\ln\rho_{A_2}\} + \frac{2}{L}\operatorname{Tr}\{\rho_{A_1}\ln\rho_{A_1}\}] \\
&= -\frac{1}{L}[\underbrace{\ln 1 + \ln 1}_{=0} + \underbrace{2\ln\frac{1}{2} + 2\ln\frac{1}{2} + \cdots + 2\ln\frac{1}{2}}_{N-1 \text{ or } \frac{L}{2}-1 \text{ total terms}}] \qquad (3.50) \\
&= (\frac{1}{L})(\frac{L}{2}-1)2\ln 2 \\
&= (\frac{L-2}{2})(\frac{2}{L})\ln 2;\ \text{recall that } L = 2N \\
S_1^{acc}(\rho_A) &= \frac{N-1}{N}\ln 2 \qquad (3.51)
\end{aligned}$$

3.2.2.2 Analytical result for any filling fraction and partition size

The analytical result obtained above for the accessible entanglement entropy in the infinitely attractive regime corresponds to the special case of half-filling ($N = \frac{L}{2}$) and equal spatial bipartitions ($\ell_A = \ell_B = \frac{L}{2}$). Nevertheless, a generalized result can be obtained for any filling fraction and partition size by counting the number of projected reduced density matrices (ρ_{A_n}) that will contribute to the accessible entanglement. As it will be shown, the number of contributing matrices will depend on how the quantities ℓ_A, ℓ_B, N & $N^c = L - N$ relate to each other. Demonstration of the following four cases will suffice to get the general result:

i) $\ell_A < N < \ell_B$

ii) $\ell_B < N < \ell_A$

iii) $N < \ell_A < \ell_B$

iv) $\ell_A < \ell_B < N$

These four cases imply other cases and, in the end, all possible relations between the four parameters will be covered.

Case *i*) $\ell_A < N < \ell_B$:

The condition here is that the size of the subregion A should be less than the total number of particles N and the size of the subregion B should be greater than both of these quantities. Under such conditions, particle configurations in which B is empty are not possible, since A is too small too fit them all. Two other configurations that will not contribute to the accessible entanglement are when A is full ($n_A = \ell_A$) and when it is empty ($n_A = 0$). There is only one possible way of distributing the particles in partition A if it is full and likewise if it is empty. As it was seen in the previous section, then the corresponding projected reduced density matrices $\rho_{A_{\ell_A}}$ and ρ_{A_0} have only one nonzero eigenvalue which, after normalization, becomes 1. Thus, $\ln \rho^{\alpha}_{A_{\ell_A}} = \ln \rho^{\alpha}_{A_0} = 0$. There are a total of $\ell_A + 1$ possible local particle numbers (n_A) and since $n_A = \ell_A$ and $n_A = 0$ do not contribute, there are actually $\ell_A - 1$ contributing projected reduced density matrices. All such projected density matrix will have the form:

$$\rho_{A_n} = \begin{pmatrix} \frac{1}{L} & 0 \\ 0 & \frac{1}{L} \end{pmatrix} \tag{3.52}$$

The two diagonal elements come from the two configurations that have the same local particle number n. Technically, these projected reduced density matrices are larger, since the basis includes configurations with all possible local particle numbers. Nevertheless, rows and columns that only have zero entries have been thrown out for compactness. Normalizing, the reduced density matrices become:

$$\rho_{A_n} = \frac{1}{P_n} \begin{pmatrix} \frac{1}{2} & 0 \\ 0 & \frac{1}{2} \end{pmatrix}; P_n = \frac{2}{L} \tag{3.53}$$

Thus, the accessible entanglement becomes:

$$S_\alpha^{acc}(\ell_A, L) = (\ell_A - 1)\frac{2}{L}\ln 2 \tag{3.54}$$

Case *ii*) $\ell_B < N < \ell_A$:

This time, partition B is the one that can never be empty. Barring that, the argument is exactly the same as *i*) and thus:

$$S_\alpha^{\text{acc}}(\ell_B, L) = (\ell_B - 1)\frac{2}{L}\ln 2 \tag{3.55}$$

Case *iii*) $N < \ell_A < \ell_B$:

In contrast to *i*) and *ii*), now the particles may all be in A or all in B. Nevertheless, in such instances, there is only a single possible configuration of the other partition, that in which it's empty. Thus, the projected reduced density matrices ρ_{A_N} and ρ_{A_0} have only one nonzero eigenvalue and, thus, do not contribute to the accessible entanglement since this eigenvalue will reduce to unity after normalization. Barring these two, there are then $N-1$ projected reduced density matrices that do contribute. They all have the same form as the ones of *i*) and *ii*), that is, $2x2$ diagonal matrices (after throwing out all unnecessary zeroes) with 2 eigenvalues equal to $\frac{1}{2}$ (after normalizing) and probabilities $P_n = \frac{2}{L}$. Thus:

$$S_\alpha^{\text{acc}}(N, L) = (N - 1)\frac{2}{L}\ln 2 \tag{3.56}$$

Case *iv*) $\ell_A < \ell_B < N$:

Here, no partition will ever be empty. The maximum allowed particle number in A is going to be $n_A = \ell_A$ and the smallest one, $n_A = N - \ell_B$. The partition size of B is subtracted from N because the minimum n_A corresponds to a fully occupied partition B, that is $n_B = \ell_B$. The 'leftover' particles on A will hence be the total particle number minus those fully occupying B. Notice

in all the previous examples that the total number of projected reduced density matrix is equal to the difference between max and min allowed particle number n_A plus 1. That is:

$$\text{Total Projected Reduced Density Matrices} = (n_A)_{max} - (n_A)_{min} + 1 \quad (3.57)$$

And for this case,

$$\begin{aligned} \text{Total Projected Reduced Density Matrices} &= (n_A)_{max} - (n_A)_{min} + 1 \\ &= \ell_A - (N - \ell_B) + 1 \\ &= \underbrace{\ell_A + \ell_B}_{L} - N + 1 \end{aligned}$$

$$\text{Total Projected Reduced Density Matrices} = L - N + 1 \quad (3.58)$$

Let $L - N \equiv N^c$. The total number of contributing projected reduced density matrices is:

$$\begin{aligned} \text{Contributing Matrices} &= \text{Total Matrices} - 2 \\ &= (N^c + 1) - 2 \\ \text{Contributing Matrices} &= N^c - 1 \quad (3.59) \end{aligned}$$

$$(3.60)$$

the accessible entanglement then becomes:

$$S_\alpha^{acc}(N^c, L) = (N^c - 1)\frac{2}{L}\ln 2 \quad (3.61)$$

The accessible entanglement at the infinitely attractive regime has now been obtained for conditions $i) - iv)$. Notice that it always has the form:

$$S_\alpha^{acc}(x, L) = (x - 1)\frac{2}{L}\ln 2 \quad (3.62)$$

where x could be ℓ_A, ℓ_B, N or N^c. But how to determine which of these variables to choose? Recalling that $L - N = N^c, L - \ell_A = \ell_B$ and $L - \ell_B = \ell_A$, extra inequalities can be obtained from $i) - iv)$ that relate the four variables:

$$
\begin{aligned}
&i) \ell_A < N < \ell_B \implies \ell_B > N^c > \ell_A \implies \ell_A \text{ is the smallest} \\
&ii) \ell_B < N < \ell_A \implies \ell_A > N^c > \ell_B \implies \ell_B \text{ is the smallest} \\
&iii) N < \ell_A < \ell_B \implies N^c > \ell_B > \ell_A \implies N \text{ is the smallest} \\
&iv) \ell_A < \ell_B < N \implies \ell_B > \ell_A > N^c \implies N^c \text{ is the smallest}
\end{aligned}
$$

From the above set of inequalities, note that the smallest between the four variables in each case, also happens to be the variable that is substituted for x. Thus, in a more compact form, the generalized operationally accessible entanglement at the infinitely attractive regime is:

$$
S_\alpha^{acc}(x, L) = \frac{2(x-1)}{L} \ln 2; \text{ where } x = \min \ell_A, \ell_B, N, N^c \tag{3.63}
$$

3.2.3 First order phase transition

At $V/t = -2$, the $t - V$ model undergoes a first order phase transition from Luttinger liquid to Phase Separated Solid. The accessible entanglement at this interaction strength vanishes and then suddenly increases and converges to the previously derived limit ($\frac{N-1}{N} \ln 2$) as the attraction gets stronger. In this section, it will be shown that the accessible entanglement vanishes at the first order phase transition.

At $\frac{V}{t} = -2$, the state of the system is an equiprobable superposition of all possible configurations (Appendix D.1). Working out the calculation of $S_1^{\text{acc}}(\rho_A)$ in matrix form, as it was done for $V/t \to \pm\infty$, turns out to be relatively complicated for this ground state. Nevertheless, reformulating the state in terms of its Schmidt decomposition gives the result almost for free. The Schmidt

decomposition of the ground state at the first order phase transition is:

$$|\Psi\rangle = \frac{1}{\sqrt{\binom{L}{N}}} \sum_{n=0}^{N} \sqrt{\binom{\ell}{n}\binom{L-\ell}{N-n}} \, |n\rangle_A \otimes |N-n\rangle_B \tag{3.64}$$

where $|n\rangle_A$ is an equal superposition of all A configurations containing n and likewise for $|N-n\rangle_B$. The square root factor inside the summation counts the number of each of the possible $|n\rangle_A \otimes |N-n\rangle_B$ configurations and the factor outside of the summation is a normalization constant. Each of the configurations, $|n\rangle_A \otimes |N-n\rangle_B$, multiplied by it's corresponding constants, represent projections of the ground state onto spaces of local particle number n. Each of these projections are separable and the contribution of each to $S_1^{\text{acc}}(\rho_A)$ is exactly zero.

To illustrate the separability of each of the projected states, the example of $N = 3$ fermions on a $L = 6$ lattice with spatial partitions of size $\ell = 3$ will be worked out. The ground state is:

$$\begin{aligned} |\Psi\rangle = \frac{1}{\sqrt{\binom{6}{3}}} [& \sqrt{\binom{3}{0}\binom{3}{3}} \, |0\rangle_A \otimes |3\rangle_B + \sqrt{\binom{3}{1}\binom{3}{2}} \, |1\rangle_A \otimes |2\rangle_B \\ & + \sqrt{\binom{3}{2}\binom{3}{1}} \, |3\rangle_A \otimes |0\rangle_B + \sqrt{\binom{3}{3}\binom{3}{0}} \, |3\rangle_A \otimes |0\rangle_B] \end{aligned} \tag{3.65}$$

Each of the terms above is a projection onto a different n subspace. Let $|\Psi_n\rangle \equiv |n\rangle_A \otimes |N-n\rangle_B$ be the projection of the ground state onto the n subspace. Technically, the square root factors are part of these projections, but they have been dropped out since they are not needed to demonstrate the separability $|n\rangle_A \otimes |N-n\rangle_B$. Expanding each projection into the site occupation basis, the projections become:

$$\begin{aligned} |\Psi_0\rangle &= |0\rangle_A \otimes |3\rangle_B = |000\rangle_A \otimes |111\rangle_B \\ &\implies S_1^{\text{acc}}(\rho_{A_0}) = 0 \end{aligned} \tag{3.66}$$

$$
\begin{aligned}
|\Psi_1\rangle = |1\rangle_A \otimes |2\rangle_B &= |100,110\rangle + |100,011\rangle + |100,101\rangle \\
&= |010,110\rangle + |010,011\rangle + |010,101\rangle \\
&= |001,110\rangle + |001,011\rangle + |001,101\rangle \\
&= (|100\rangle + |010\rangle + |001\rangle)_A \otimes (|110\rangle + |011\rangle + |101\rangle)_B \\
&\implies S_1^{\text{acc}}(\rho_{A_1}) = 0
\end{aligned} \tag{3.67}
$$

$$
\begin{aligned}
|\Psi_2\rangle = |2\rangle_A \otimes |1\rangle_B &= |110,100\rangle + |110,010\rangle + |110,001\rangle \\
&= |011,100\rangle + |011,010\rangle + |011,001\rangle \\
&= |101,100\rangle + |101,010\rangle + |101,001\rangle \\
&= (|110\rangle + |011\rangle + |101\rangle)_A \otimes (|100\rangle + |010\rangle + |001\rangle)_B \\
&\implies S_1^{\text{acc}}(\rho_{A_2}) = 0
\end{aligned} \tag{3.68}
$$

$$
\begin{aligned}
|\Psi_0\rangle = |3\rangle_A \otimes |0\rangle_B &= |111\rangle_A \otimes |000\rangle_B \\
&\implies S_1^{\text{acc}}(\rho_{A_3}) = 0
\end{aligned} \tag{3.69}
$$

Note that $S_1(\rho_{A_n}) = 0, \forall\ n \in \{0,1,2,3\}$. Thus,

$$
S_1^{\text{acc}}(\rho_A) = \sum_{n=0}^{3} P_n S_1(\rho_{A_n}) = 0 \tag{3.70}
$$

The von Neumann accessible entanglement vanishes at the first order phase transition. The above behavior is exhibited for any system size and it is also independent of the partition size.

3.3 Comparison between the accessible Rényi and von Neumann entanglement entropies

Recall the generalized form of the Rényi accessible entanglement entropy:

$$S_\alpha^{\mathrm{acc}}(\rho_A) = \frac{\alpha}{1-\alpha} \ln \left[\sum_n P_n \mathrm{e}^{\frac{1-\alpha}{\alpha} S_\alpha(\rho_{A_n})} \right] \tag{3.71}$$

In the previous section, the von Neumann accessible entanglement was calculated for $V/t \to -\infty, V/t \to +\infty$ and $V/t = -2$. Analogous derivations can be done for the accessible Rényi entanglement entropy Eq. (3.71). Here, the results for the Rényi and von Neumann accessible entanglement are summarized

Interaction	$S_\alpha^{\mathrm{acc}}(\rho_A) = \frac{\alpha}{1-\alpha} \ln \left[\sum_n P_n \mathrm{e}^{\frac{1-\alpha}{\alpha} S_\alpha(\rho_{A_n})} \right]$	$S_1^{\mathrm{acc}}(\rho_A) = \sum_n P_n S_1(\rho_{A_n})$
$V/t \to -\infty$	$\frac{\alpha}{1-\alpha} \left[\frac{2(x-1)}{L} 2^{\frac{1-\alpha}{\alpha}} + 1 - \frac{2(x-1)}{L} \right]$	$\frac{2(x-1)}{L} \ln 2$
$V/t \to +\infty$	$\ln 2$ if N even, 0 if N odd	$\ln 2$ if N even, 0 if N odd
$V/t = -2$	0	0

Table 3.1: Analytical results for the accessible entanglement in the ground state of the $t-V$ model with N fermions on L sites under a spatial bipartition consisting of $\ell = L/2$ contiguous sites. From left to right, the columns indicate the interaction strength, the value of the generalized Rényi accessible entanglement, and the value of the von Neumann entanglement, respectively. The x in the first row is the minimum value between $\{N, \ell, L-\ell, L-N\}$.

Analytical results have now been obtained in three regimes of the $t-V$ Model, namely: $V/t \to +\infty$, $V/t \to -\infty$ and $V/t = -2$ for both the von Neumann and the Rényi accessible entanglement. In the next section, numerical results obtained from exact diagonalization are presented.

3.4 Numerical Results

3.4.1 Finite size scaling of the accessible entanglement

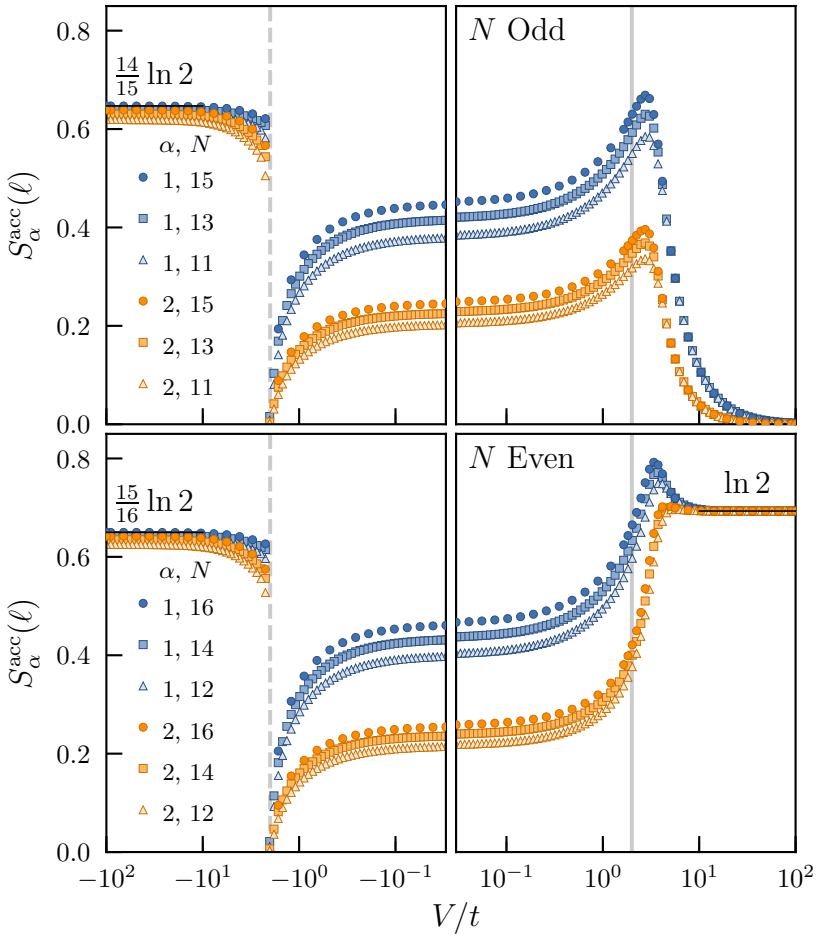

Figure 3.1: Accessible entanglement entropy $S_\alpha^{\mathrm{acc}}(\ell)$ for $\alpha = 1, 2$ in the ground state of the $t-V$ model as a function of interaction strength V/t. The top panel shows the results for an odd number of total particles: $N = 11, 13, 15$ and the bottom, for even: $N = 12, 14, 16$. The gray vertical lines indicate the locations of the known phase transitions for the model, $V/t = \pm 2$. For $N = 15, 16$ the asymptotic results computed in Section 3.1 in the limits $V/t \to \pm\infty$ for S_1^{acc} are shown.

Figure 3.1 shows the accessible Rényi entanglement entropy values at interaction strengths in the interval $V/t : (-100, 100)$. This interval spans the three phases of the $t - V$ model. For large negative interaction strengths, there is agreement between the values at which $S_\alpha^{\mathrm{acc}}(\rho_A)$ converges and the predicted value from 3.1 for all system sizes and α. For large positive inter-

action strengths, the predicted effect of total particle number parity is observed. For N odd, the accessible entanglement vanishes, whereas it converges to $\ln 2 \approx 0.6931\ldots$ for N even, independent of system size and α. At the first order phase transition $V/t = -2$, $S_\alpha^{\text{acc}}(\rho_A)$, as expected. Thus, the asymptotic predictions for the accessible entanglement entropy in the $t - V$ model have been confirmed via exact diagonalization. Increasing the magnitude of both the attractive and repulsive interactions will result in even more agreement between simulation and theory.

Recall that the accessible entanglement should be a monotonically decreasing function of α. Figure 3.1 supports this inverse relation since it is seen that $S_1 \geq S_2 \; \forall \; V/t \in (-100, 100)$.

Another interesting feature is the peak seen near the continuous phase transition $V/t = 2$. Results seem to indicate that the peak is slightly shifting to the left, closer to $V/t = 2$ as the number of particles N increases. In an effort to find how the location of this peak scales with particle number, $V/t|_{Max}$ was obtained for various system sizes, where $V/t|_{Max}$ is the interaction strength at which the accessible entanglement peak occurs. Figure 4.2 shows a plot of $V/t|_{Max}$ vs $N^{-0.2545}$. The exponent comes from a linear fitting of $(V/t|_{Max} - 2)$ vs N data. The observed inverse power law scaling is promising as all points fall on a line with y intercept of $V/t|_{Max} = 2$, which is the exact value of the continuous phase transition in the asymptotic limit of $N \to \infty$ total particles. Nevertheless, most of the system sizes in the data fall roughly in the same order of magnitude. The exact value of the phase transition $V/t = 2$ is obtained in the thermodynamic limit of $N \to \infty$ particles. Thus, to confirm the veracity of a power-law scaling of the peak of entanglement, more data points will be needed. Deviations from the line are noticeable in the largest three points presented. This suggests that there might be sub-leading terms that will hopefully become negligible for large system sizes. Currently, data for larger system sizes is being generated via Density Matrix Renormalization Group (DMRG) that

will allow for the simulation of $N \approx 100$ fermions [63] .

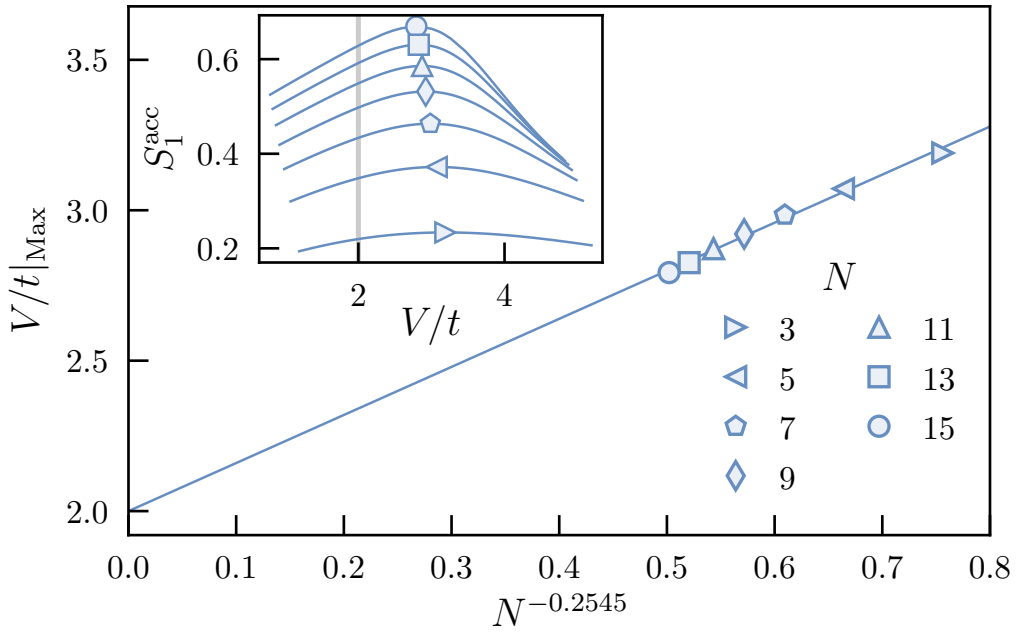

Figure 3.2: Interaction strength at which the maximum S_1^{acc} occurs as a function of the total number of particles N. The exponent of N was obtained from a linear fitting of $\ln N$ vs. $\ln(V/t - 2)$. Although very few points are plotted due to memory limitations, they agree with the hypothesis that for $N \to \infty$, the peak of von Neumann accessible entanglement occurs at the phase transition $V/t = 2$. Inset: S_1^{acc} as a function of interaction strength V/t for various N around the neighborhood of the peak.

3.4.2 Entanglement of local particle number fluctuations

Recall from section 3.1.1 that the difference between the full and the operationally accessible von Neumann entropies ($\alpha = 1$) should equal the Shannon entropy of the local particle number probability distribution P_n:

$$\Delta S_1(\rho_A) \equiv S_1(\rho_A) - S_1^{\mathrm{acc}}(\rho_A) = H_1(\{P_n\}) \tag{3.72}$$

where

$$H_1(\{P_n\}) = -\sum_{n=0}^{N} P_n \ln P_n. \tag{3.73}$$

is the Shannon entropy of the probability distribution of the local particle number P_n.

In this section, a comparison is done between the Shannon entropy of the local particle number distribution and the difference between full and accessible entanglement. First, numerical results for this difference will be shown for the case of $\alpha = 1$ and compared to the exact value of the Shannon entropy of normally distributed local particle numbers. Then, higher values of α will be studied and the difference will be compared with the Shannon entropy of the corresponding probability distribution of local particle number.

Figure 3.3 shows the difference between the full and accessible von Neumann entanglement entropies as a function of interaction strength. From exact diagonalization, the full (S_1), accessible (S_1^{acc}) von Neumann entanglement entropies and the variance of local particle number n (σ) were obtained. Expecting that local particle number fluctuations are normally distributed in the TLL phase ($-2 < V/t < 2$) of the $t - V$ model, these variances were inserted into the expression for the Shannon entropy of a Normal Distribution $\frac{1}{2}\ln(2\pi e\sigma^2)$. Additionally, the Shannon entropy was calculated using the variance of local particle number predicted by Tomonaga-Luttinger Liquid theory $\sigma \equiv K\sigma_{FF}$ where σ_{FF} is the variance of free-fermions $V/t = 0$ and K is the Luttinger Parameter $K = \pi/(\cos^{-1}(-V/2t))$, as shown in Chapter 2 . The figure shows agreement between the three expressions in the TLL phase.

At Rényi indices higher than $\alpha = 1$, the difference between the full and accessible entanglement entropies should be bounded from below by the classical Rényi entropy of the local particle number probability distribution $H_\alpha(\{P_n\}) = \ln\sum_n P_n^\alpha/(1-\alpha)$. Figure 3.4 shows ΔS_α and $H_\alpha(\{P_n\})$ as a function of interaction strength for Rényi indices $\alpha = 2$ and $\alpha = 10$. Not only in all cases is $H_\alpha(\{P_n\}) \leq \Delta S_\alpha$, but also the values corresponding to $\alpha = 10$ are lower than the ones corresponding to $\alpha = 2$, satisfying the condition that the difference in full and accessible entanglement should be a monotonically decreasing function

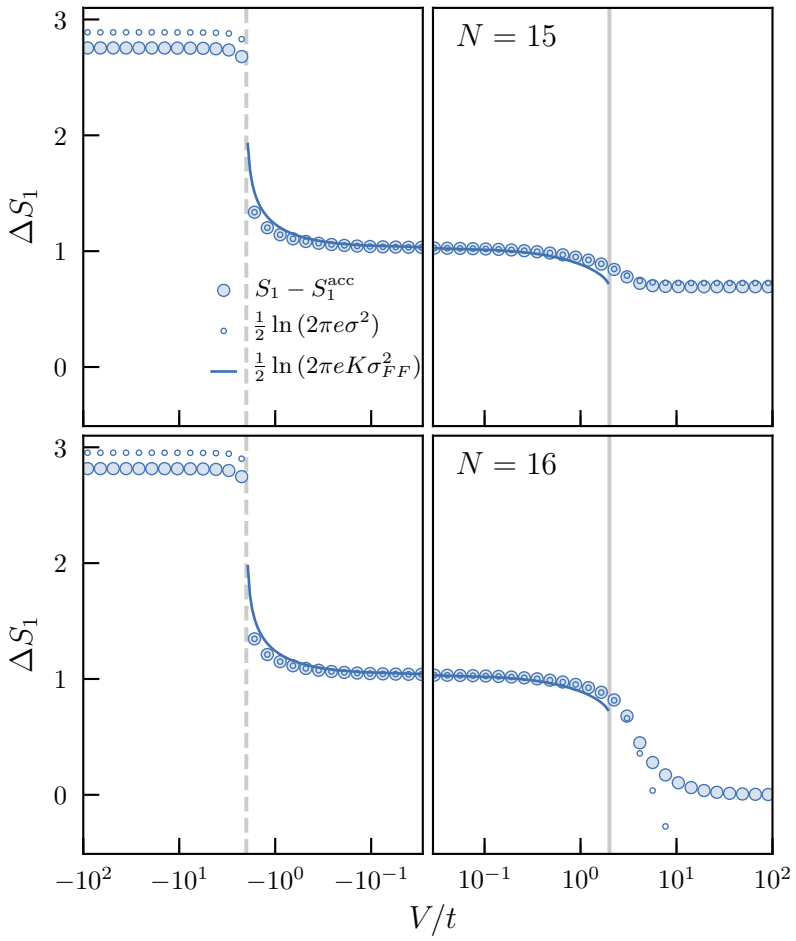

Figure 3.3: Difference between the von Neumann and accessible entanglement entropies $S_1 - S_1^{acc}$ and $\frac{1}{2}\ln 2\pi e\sigma^2$ as functions of interaction strength V/t. The latter expression is the well known differential entropy of a Gaussian distribution. In TLL phase ($-2 < V/t < 2$), the probability distribution is Gaussian, as can be seen from the agreement between the two results. The solid lines use the theoretical variance of particle number in A inside the LL phase, $K\sigma_{FF}^2$, where K is the Luttinger parameter and is a function of V/t and σ_{FF}^2 is the exact variance for free-fermions ($V/t = 0$).

of α. The fact there's such good agreement for the $\alpha = 2$ and $\alpha = 10$ is rather astounding. Taking a look at Figure 3.5 reveals that the difference between the computationally determined Rényi entropy of P_n and the theoretical value is proportional to the Rényi index. For $\alpha = 10$, this difference is large enough that the agreement in the TLL phase in Figure 3.4 is surprising. Up next, it will be shown that this agreement is a result of the proportionality between $P_{n,\alpha}$ and P_n^α.

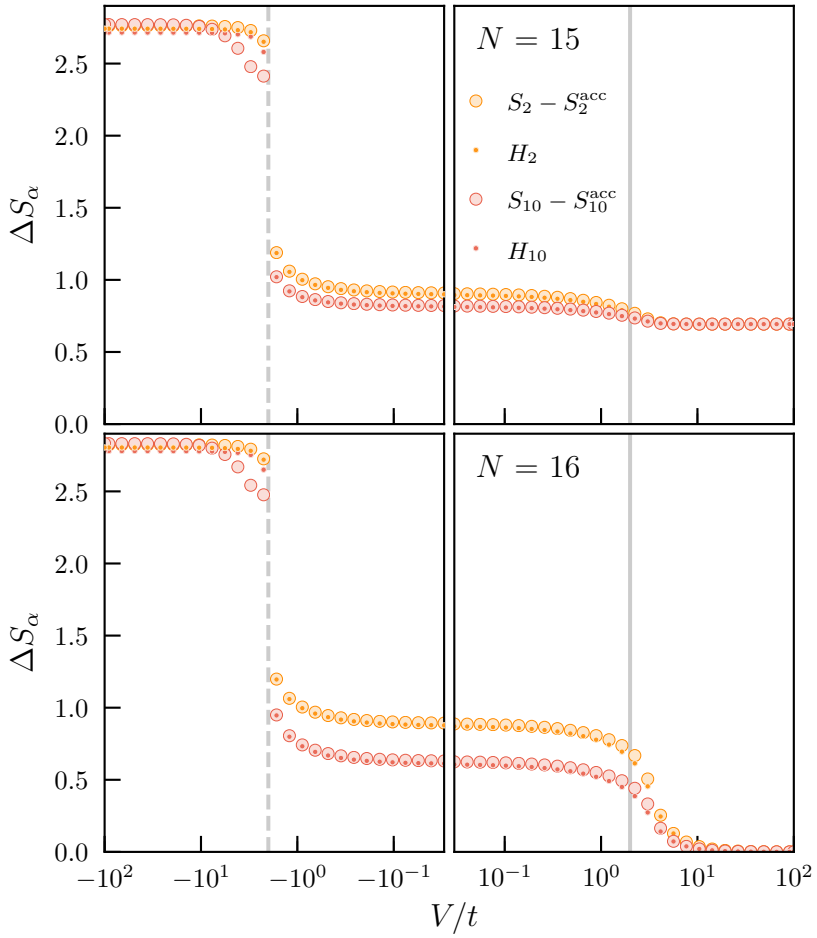

Figure 3.4: Difference between the Rényi and accessible entanglement entropy $S_\alpha - S_\alpha^{\mathrm{acc}}$ and H_α as functions of interaction strength V/t for $\alpha = 2, 10$. In general, H_α should provide a lower bound for ΔS_α (i.e, $H_\alpha \leq S_\alpha$). Also, S_α^{acc} should be non-increasing in α. It can be seen that both relations hold in all phases of the $t - V$ model.

Recall the distribution defined in section 3.1.1:

$$P_{n,\alpha} = \frac{P_n}{\mathrm{Tr}\,\rho_A^\alpha} \tag{3.74}$$

which due to a normal distribution of local particle numbers in the TLL phase of the $t - V$ model ($-2 < V/t < 2$) can be approximated as:

$$P_{n,\alpha} \approx \sqrt{\frac{\pi\alpha}{2K \ln \ell}} e^{\frac{-\alpha\pi^2(n-\langle n\rangle^2)}{2K \ln \ell}} \tag{3.75}$$

Notice that raising Eq. (3.75) to either $1/\alpha$ or K on both sides should get

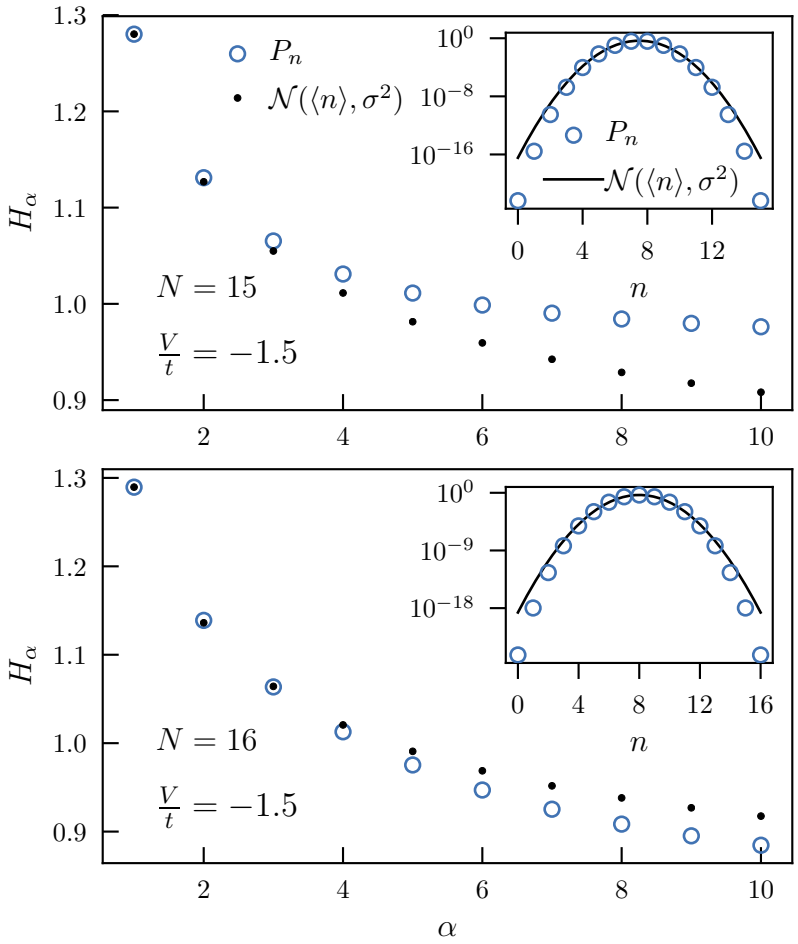

Figure 3.5: For $N = 15$, $\sigma^2 = 0.758$ and for $N = 16$, $\sigma^2 = 0.772$.

rid of the α or K dependence of the exponential factor, respectively, within the TLL regime. The square root factor will still pick up the dependence on either of the exponents. In other words, raising by $1/\alpha$ or K should give:

$$P_{n,\alpha}^{1/\alpha} \approx \sqrt{\frac{\pi\alpha}{2K\ln\ell}}^{1/\alpha} e^{\frac{-\pi^2(n-\langle n\rangle^2)}{2K\ln\ell}} \tag{3.76}$$

and

$$P_{n,\alpha}^{K} \approx \sqrt{\frac{\pi\alpha}{2K\ln\ell}}^{K} e^{\frac{-\alpha\pi^2(n-\langle n\rangle^2)}{2\ln\ell}} \tag{3.77}$$

Figure 3.6 shows the distribution $A_\alpha P_{n,\alpha}^{1/\alpha}$ for various interaction strengths V/t and, thus, K. The constant A_α is the inverse of the square root factor in

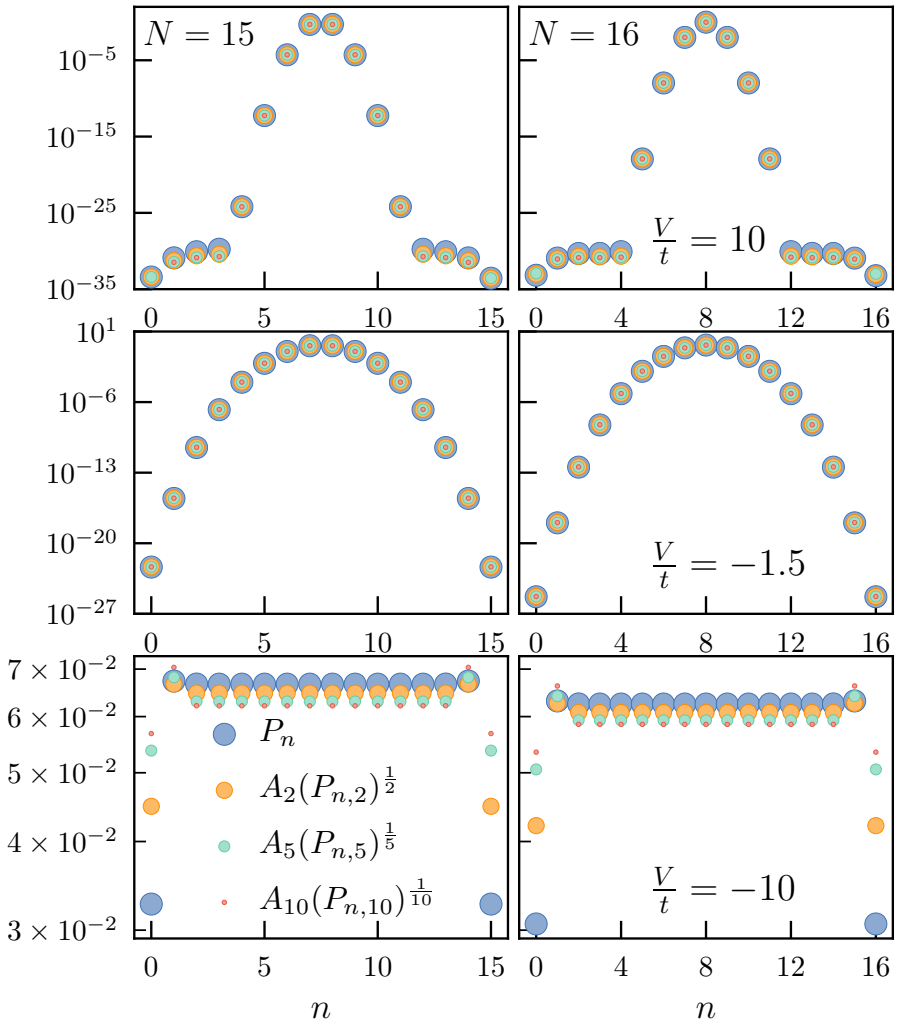

Figure 3.6: Probabilities of measuring a state with n particles in subregion A, as a function of n. The probabilities in the TLL regime are known to be Gaussian. Here, they have been raised to $1/\alpha$ in order to cancel out the α dependence of the exponential part. For the middle plot, the interaction strength lies in the TLL regime and, consequently, the probabilities collapse to the same values in all the range after the α dependence has been cancelled. The top and bottom plots show results outside of the TLL regime, where the probabilities are not Gaussian.

Eq. (3.76). Cancelling the square root factor allows for a direct comparison of the exponential factor for each of the α values used. The middle plots confirm that this exponential factor indeed is independent of α, illustrated by the fact that the distributions become the same for $\alpha = \{1, 2, 5, 10\}$, when inside the TLL regime of $-2 < V/t < 2$.

Figure 3.7 shows the distribution $A_\alpha P^K_{n,\alpha}$ with the Rényi index fixed at

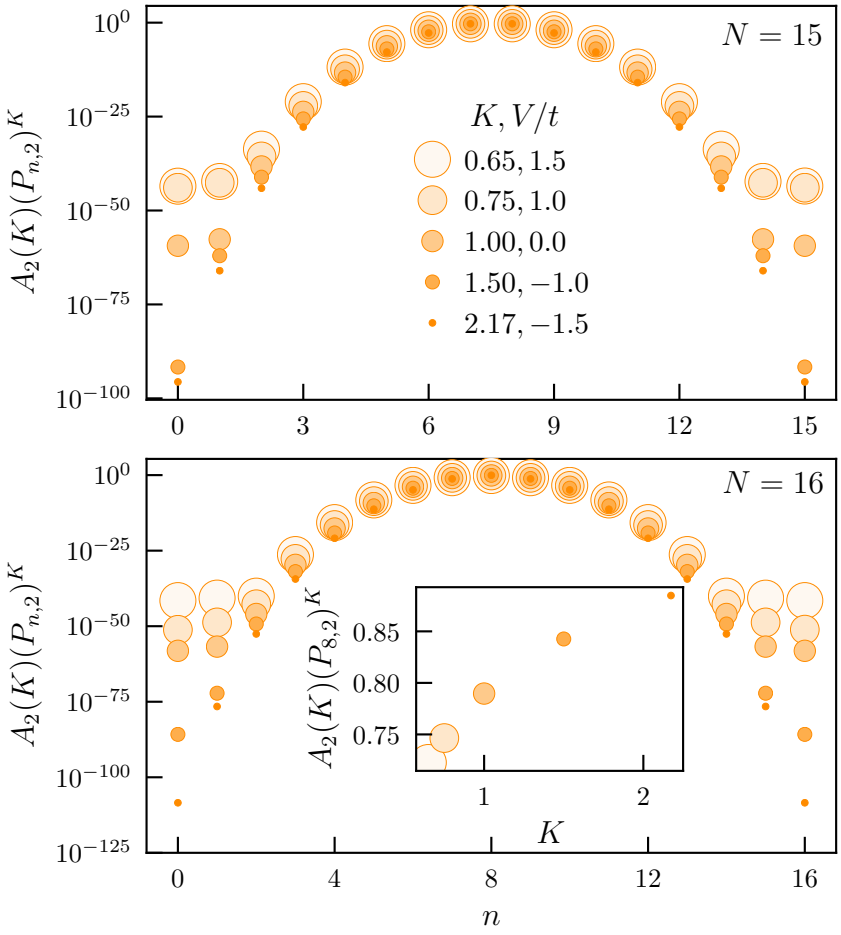

Figure 3.7: Probabilities of measuring a state with n particles in subregion A, as a function of n. This time, the probabilities have been raised to the Luttinger Parameter K, after calculating for several K values. The probabilities seem to collapse nearly to the same value near the middle of the distribution. The inset plot shows the K dependence of the probability for fixed particle number in A, $n = 8$. This helps illustrate that the probabilities are proportional to K near the middle, as opposed to inversely proportional at the ends.

$\alpha = 2$ and at various interaction strengths V/t and corresponding Luttinger parameters K. In this case, the factor A_α is the inverse of the square root factor in Eq. (3.77). All of the interaction strengths fall within the TLL regime and as such, all the distributions should become the same for the various V/t and, thus, K values. This collapse of the distributions at various K is evident from looking at regions near the middle of the graph. Although it may not be apparent at first glance due to the scale, the tails of the distribution are all essentially zero.

3.5 Conclusion

In this chapter, the operationally accessible Rényi entanglement entropy was introduced in both it's original and generalized form. Analytical values of the entanglement entropy were obtained at various special cases of the $t-V$ model and then confirmed via exact diagonalization. A maximum value in accessible entanglement was observed and evidence seems to support that it follows an inverse power law scaling in total particle number with scaling exponent -0.2545.

The difference in full and accessible entanglement entropies was also computationally determined and it was confirmed that in the TLL phase of the $t-V$ model, it is equal to the the Rényi entropy of a Normal Distribution of local particle number. Finally, it was then proposed theoretically and confirmed computationally, that getting rid of its Rényi index and Luttinger parameter dependence, the exponential part of these Normal Distributions depend exclusively on local particle number fluctuations.

Chapter 4

Conclusions and Future Work

4.1 Conclusions

4.1.1 Particle entanglement of one-dimensional spinless fermions

The empirical scaling form for the one-particle entanglement entropy in the $t-V$ model proposed in [24] was confirmed analytically. This scaling suggested that the one-particle entanglement entropy should go as $S(n,N) = \ln\binom{N}{n} + a + \mathcal{O}(\frac{1}{N^\gamma})$, where n is the number of particles in the subsystem, N is the total number of particles in the system, and a and γ are parameters that depend on the interaction between the fermions and hence the Luttinger Parameter, K. The first term on the scaling form is the free-fermion contribution to the entanglement entropy. Having confirmed analytically the empirically proposed scaling of the one-particle entanglement entropy, the entanglement contribution coming from particle interactions was calculated. To calculate the particle interaction contribution to the one-particle entanglement entropy, $S(n,N) - \ln\binom{N}{n}$ was calculated at various values of particle interaction strengths V/t. Not only agreement was again seen between numerical results, Tomonaga-Luttinger Liquid (TLL) theory and the proposed scaling, but it was also seen that the

one-particle entropy was sensitive to phase transitions in the $t - V$ model.

4.1.2 Accessible spatial entanglement entropy of one-dimensional spinless fermions

The amount of spatial entanglement in the $t - V$ model that is accessible as a resource was computed analytically and via exact diagonalization as a function of interaction strength. It was seen that this type of entanglement was also sensitive to the phase transitions of the model. At the continuous phase transition, a peak was observed and a power-law scaling suggests that in the limit of inifitely many fermions, this peak would move exactly to the value of the phase transition. The difference between the full and the accessible entanglement entropies was also computed. Also via exact diagonalization, it was confirmed that the probabilities of measuring a number n of particles are Gaussianly distributed.

4.1.3 Summary

This work confirmed the effectiveness of quantum entanglement as a probe for quantum phase transition.

It was also seen that the way a system is partitioned will give different insights into the entanglement of a system. Partitioning a system into spatial subregions gives insight into how information is shared across the boundary between the regions. On the other hand, a particle partition gives a length-scale free and particle-statistics dependent idea of how information is shared between entangled groups of particles. The entanglement under both of these types of partitions was used to successfully detect phase transitions in the $t-V$ model. Features were seen using one type of entanglement that were not seen with the other. For example, for particle entanglement, it was seen how the von Neumann and Rényi entropies had a contribution due to fermionic statistics,

while the spatial entanglement showed a peak of entanglement at the continuous phase transition that scales with system size. The ability of each partition type to capture different features of the systems means that that future studies should focus on measuring both, in order to give a broader understanding of the particular model under studied.

-The type of partition can give different insights (particle part depends on statistics, it is independent of length scales, perhaps it is more pure)

-Superselection rules will give a better understanding of the entanglement that can be used (for quantum computing, for example)

4.2 Future work

In this section, future projects are discussed. Some of these projects stem from unanswered questions in previous work, while some of them will be completely new.

4.2.1 Power law scaling of entanglement peak in the tV model

In the $t-V$ model, there are two known phase transitions, a first order one at $V/t=-2$, and a continuous one at $V/t=2$. From Figure 4.1, it can be seen that the accessible entanglement entropies are sensitive to both types of transition. Interestingly, this sensitivity to the transition in $V/t=2$ expresses itself as a peak of entanglement. Moreover, the interaction strength at which this peak of entanglement occurs moves closer to the exact value of the continuous phase transition as the number of particles in the system increases.

Figure 4.2 shows the value where the entanglement peak occurs for various system sizes. The fact that all the points lie on a line that intercepts the vertical axis at $V/t_{Max}=2$ is very promising. Nevertheless, the current scaling

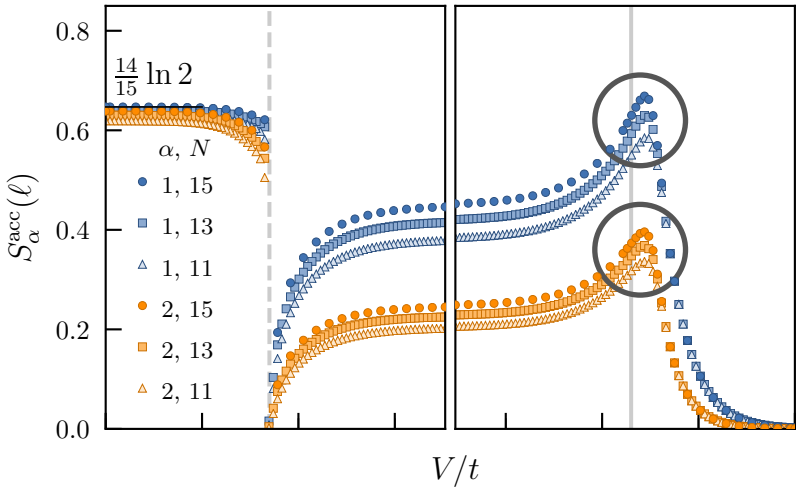

Figure 4.1: Accessible entanglement entropies as a function of interaction strength in the $t-V$ model. The circles enclose a region where both the von Neumann and Rényi entanglement entropies attain a maximum value. As the total number of particles N increases, this maximum seems to be shifting to the left, closer to the phase transition $V/t = 2$.

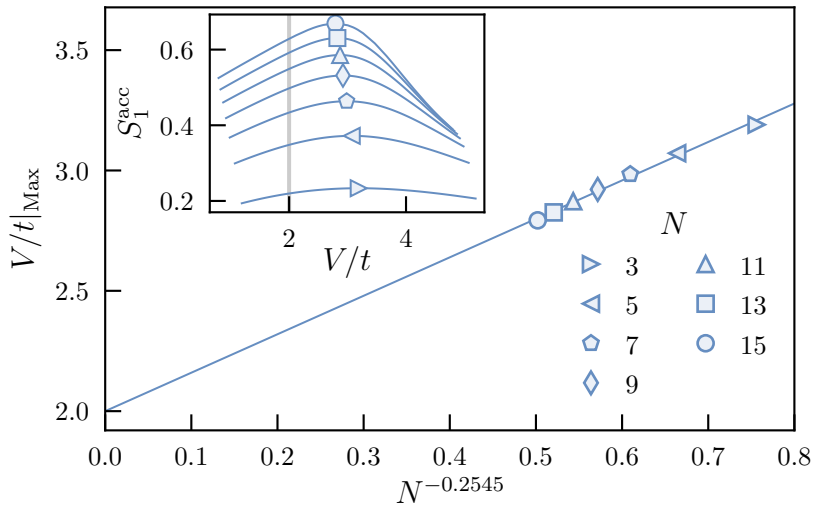

Figure 4.2: Interaction strength at which the maximum S_1^{acc} occurs as a function of the total number of particles N. The exponent of N was obtained from a l inear fitting of $\ln N$ vs. $\ln(V/t-2)$. Although very few points are plotted due to memory limitations, they agree with the hypothesis that for $N \to \infty$, the peak of von Neumann accessible entanglement occurs at the phase transition $V/t = 2$. Inset: S_1^{acc} as a function of interaction strength V/t for various N around the neighborhood of the peak.

exponent of -0.2545 should not be taken for granted due to how small the systems currently are. Indeed, the continuous phase transition should occur in

the $t - V$ model at $V/t = 2$, but this is for a system where $N \to \infty$. More data points, corresponding to large systems are still be needed to get closer to this intercept and confirm the power law scaling. To aid in reaching this larger system sizes, Density Matrix Renormalization Group (DMRG) will be employed [63, 64]. With DMRG, it is expected that systems consisting of roughly 100 particles can be simulated.

4.2.2 Filling fraction dependence of entanglement

The $t - V$ model results presented in this thesis were focused on the special case of half-filling. That is, only half of the lattice sites were had particles in them ($N = L/2$). For this case, the exact results for the phase transitions are mapped from the XXZ spin-1/2 model. For other filling fractions, a theory has yet to be developed. Figure 4.3 shows the accessible entanglement entropies for various filling fractions ranging from 1/14 to 1/2. Expanding the results outside the realm of half filling will help to learn if some of the interesting features observed, such as the scaling of the accessible entanglement peak and the Gaussian distribution of local particle number probabilities in the TLL phase, are independent of filling fraction.

4.2.3 Accessible entanglement via quantum gates

The endgame for the study of accessible entanglement entropies is to exploit the entanglement of a system as a resource. Motivated by this, we are currently working on building a quantum circuit that reproduces the accessible entanglement measurement process. After coming up with the appropriate quantum circuit, the results will be tested on IBM's quantum computer [65].

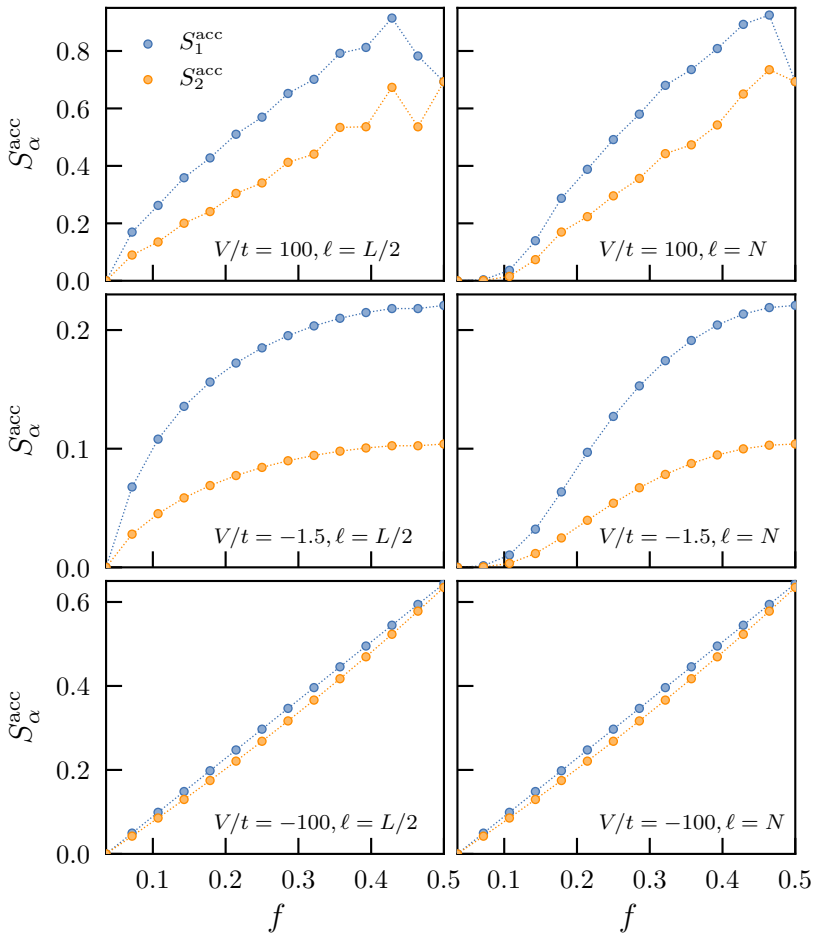

Figure 4.3: Accessible entanglement entropies $S_\alpha^{\rm acc}(\ell)$ for $\alpha = 1, 2$ as a function of filling fraction N/L. The lattice size was kept fixed at $L = 28$ sites and the total number of particles were $N = 1, 2, 3...14$. For the left column, the spatial partition ℓ was kept fixed at half the lattice size, $\ell = L/2$. For the right column, it was set to equal the total number of particles N. The interaction strengths V/t are indicated in each of the plots and correspond to values from each of the three phases of the $t - V$ model.

4.2.4 Entanglement in the Bose-Hubbard model

Another project in the works is calculating accessible entanglement entropies in the Bose-Hubbard (BH) model. In the study of fermionic systems, such as the $t - V$ model, methods like exact diagonalization and density matrix renormalization group must be used to due to the infamous sign problem. The high memory cost of these methods restricts simulations to only relatively small system sizes and low dimensions. The sign problem does not exist in bosonic

models and thus quantum Monte Carlo (QMC) methods can be used. QMC will allow the study of much larger systems than the ones presented here [1, 66].

Appendix A

A.1 Site to momentum basis mapping of kinetic operator

The kinetic energy operator of the fermionic $t-V$ Model is:

$$\hat{T} = -t \sum_i c_i^\dagger c_{i+1} + h.c$$

where t is the hopping amplitude, c_i ($c_i^\dagger$) is the fermionic annihilation (creation) operator on site i, $h.c$ stands for "Hermitian Conjugate" and the sum is carried over all lattice sites. This operator describes a fermion hopping between neighboring sites. Nevertheless, it may not be obvious in a physical sense how this expression 'counts' the contribution to the kinetic energy in the model. Here it will be shown that:

$$-t \sum_i c_i^\dagger c_{i+1} + h.c = \sum_k \epsilon(k) n_k$$

where $\epsilon(k)$ is the dispersion relation of a fermion with momentum $p_k = \hbar k$ and n_k counts how many fermions have wavenumber k. Hopefully, the expression on the right makes conceptually clearer how the kinetic energy operator is actually counting the total kinetic energy of a state. To move from real space to $k-space$, the discrete version of the Fourier Transform will be applied to

the fermionic creation and annihilation operators.

Consider a lattice with L total sites. The Discrete Fourier Transform (DFT) is defined as:

$$f_j = \frac{1}{\sqrt{L}} \sum_k f_k e^{ikj}$$

The index j has been chosen to represent the lattice sites in order to avoid confusion with the imaginary unit, i.

Thus, applying the DFT to the creation and annihilation operators:

$$c_j^\dagger = \frac{1}{\sqrt{L}} \sum_k e^{-ikj} c_k^\dagger$$

$$c_j = \frac{1}{\sqrt{L}} \sum_k e^{ikj} c_k$$

Now, consider the first term of the kinetic operator (without the $-t$, for now) and substitute these 'transformed' operators:

$$\begin{aligned}
\sum_j c_j^\dagger c_{j+1} &= \sum_j [\frac{1}{\sqrt{L}} \sum_k e^{-ikj} c_k^\dagger \frac{1}{\sqrt{L}} \sum_{k'} e^{ik'(j+1)} c_{k'}] \\
&= \frac{1}{L} \sum_j [\sum_k \sum_{k'} c_k^\dagger c_{k'} e^{i(k'-k)j} e^{ik'}] \\
&= \sum_k \sum_{k'} c_k^\dagger c_{k'} e^{ik'} \underbrace{\frac{1}{L} \sum_j e^{i(k'-k)j}}_{\stackrel{def}{=} \delta_{kk'}} \\
&= \sum_k \sum_{k'} c_k^\dagger c_{k'} e^{ik'} \delta_{kk'}; \text{ only the k'=k term 'survives'} \\
\sum_j c_j^\dagger c_{j+1} &= \sum_k c_k^\dagger c_k e^{ik}
\end{aligned}$$

The Hermitian Conjugate of this gives the second term in the operator. It is obtained almost for free from the above result:

$$\sum_j c_{j+1}^\dagger c_j = \sum_k c_k^\dagger c_k e^{-ik}$$

Adding the last two lines and multiplying by (minus) the hopping amplitude t:

$$\begin{aligned}
-t\sum_j [c_j^\dagger c_{j+1} + c_{j+1}^\dagger c_j] &= -t\sum_k [c_k^\dagger c_k e^{ik} + c_k^\dagger c_k e^{-ik}] \\
&= -t\sum_k [c_k^\dagger c_k (e^{ik} + e^{-ik})] \\
&= -t\sum_k [c_k^\dagger c_k (2\cos(k))] \\
&= \sum_k [\underbrace{c_k^\dagger c_k}_{n_k} \underbrace{(-2t\cos(k))}_{\epsilon(k)}]
\end{aligned}$$

Therefore:

$$\hat{T} = -t\sum_j [c_j^\dagger c_{j+1} + c_{j+1}^\dagger c_j] = \sum_k \epsilon(k) n_k$$

Q.E.D

On a side note, the dispersion relation for fermions on a one dimensional lattice with lattice constant a is: $\epsilon(k) = -2t\cos(ka)$, which was retrieved here for $a = 1$.

Appendix B

B.1 Lanczos Algorithm

B.1.1 Introduction

The Lanczos Algorithm, takes as input a Hermitian Matrix and iteratively builds a similarity transform that makes it tridiagonal. Due to similarity, the solution of the eigenvalue problem of the tridiagonal matrix is the same as that of the original matrix. Nevertheless, some methods can exploit the tridiagonality to find the eigendecomposition more easily. In condensed matter physics, the input matrix is usually a Hamiltonian. The eigenvalues and eigenvectors of the Hamiltonian represent the energies and the associated quantum states of the system.

In the following section, the Lanczos Algorithm will be derived. Next, some methods for approximating the eigenvalues and eigenvectors will be discussed. Finally, a hopefully simple implementation of the algorithm in Python will be linked and some results will be shown.

B.1.2 Tridiagonalization of the original matrix

Let A be a Hermitian matrix of size $n \times n$. An orthonormal transform matrix Q is needed such that:

$$T = Q^T A Q \tag{B.1}$$

where T is a tridiagonal and Hermitian matrix similar to A.

The idea is to obtain a recursive relation, starting from the known fact that T is tridiagonal and that the columns of the transform Q are mutually orthonormal. The matrix T has the form:

$$T = \begin{pmatrix} \alpha_1 & \beta_1 & & & & & 0 \\ \beta_1 & \alpha_2 & \beta_2 & & & & \\ & \beta_2 & \alpha_3 & \beta_3 & & & \\ & & \beta_3 & \ddots & \ddots & & \\ & & & \ddots & \alpha_{n-2} & \beta_{n-2} & \\ & & & & \beta_{n-2} & \alpha_{n-1} & \beta_{n-1} \\ 0 & & & & & \beta_{n-1} & \alpha_n \end{pmatrix} \tag{B.2}$$

Operating Q on both sides of the similarity relation above from the left:

$$QT = QQ^T AQ = IAQ = AQ \tag{B.3}$$

Let $\{q_1, q_2, q_3, ..., q_k\}$ be represent the mutually orthonormal columns of Q and $\{t_1, t_2, t_3, ..., t_k\}$, those of T. Then, at the k-th step of the Lanczos iteration:

$$Aq_k = Qt_k \tag{B.4}$$

$$= \begin{pmatrix} \cdots & q_{1,k-1} & q_{1,k} & q_{1,k+1} & \cdots \\ \cdots & q_{2,k-1} & q_{2,k} & q_{2,k+1} & \cdots \\ & & \vdots & & \\ \cdots & q_{n,k-1} & q_{n,k} & q_{n,k+1} & \cdots \end{pmatrix} \begin{pmatrix} \vdots \\ 0 \\ \beta_{k-1} \\ \alpha_k \\ \beta_k \\ 0 \\ \vdots \end{pmatrix} \tag{B.5}$$

The column vector only has three nonzero components. Namely, β_{k-1}, α_k and

β_k. Thus, the product of this matrix-vector multiplication becomes:

$$Aq_k = \begin{pmatrix} q_{1,k-1} \\ q_{2,k-1} \\ \vdots \\ q_{n,k-1} \end{pmatrix} \beta_{k-1} + \begin{pmatrix} q_{1,k} \\ q_{2,k} \\ \vdots \\ q_{n,k} \end{pmatrix} \alpha_k + \begin{pmatrix} q_{1,k+1} \\ q_{2,k+1} \\ \vdots \\ q_{n,k+1} \end{pmatrix} \beta_k \tag{B.6}$$

$$\tag{B.7}$$

Or, more compactly:

$$Aq_k = \beta_{k-1}q_{k-1} + \alpha_k q_k + \beta_k q_{k+1} \tag{B.8}$$

From this three-term recursion relation, Q can be built by finding equations for the nonzero elements of the set of columns $\{q_i\}_{i=1}^n$ (i.e the α's and β's). First, the α_k equation will be derived. Multiplying both sides of the three-term recursion relation by q_k^T from the left:

$$q_k^T Aq_k = \beta_{k-1}q_k^T q_{k-1} + \alpha_k q_k^T q_k + \beta_k q_k^T q_{k+1} \tag{B.9}$$

Since the columns of Q are mutually orthonormal, $q_k^T q_{k'} = \delta_{kk'}$. In other words, the first and third term will vanish and the second one survives. The equation for α_k is then:

$$\alpha_k = q_k^T Aq_k \tag{B.10}$$

To obtain the β_k equation, first the recursion relation is solved for $\beta_k q_{k+1}$, which gives:

$$\beta_k q_{k+1} = Aq_k - \alpha_k q_k + \beta_{k-1}q_{k-1} = (A - \alpha_k I)q_k - \beta_{k-1}q_{k-1} \tag{B.11}$$

Setting $r_k \equiv (A - \alpha_k I)q_k - \beta_{k-1}q_{k-1}$:

$$\beta_k q_{k+1} = r_k \tag{B.12}$$

Or

$$q_{k+1} = \frac{r_k}{\beta_k} \tag{B.13}$$

where $\beta_k \neq 0$ and, since q_{k+1} is an orthonormal vector, $\beta_k = ||r_k||_2$, such that q_{k+1} is normalized.

Note that the α_k and β_k terms of the three-term recursion relation have been accounted for. As for the β_{k-1}, a "bottom rung" for the recursion has to be set. The tridiagonal matrix T does not have a β_{k-1} term. Thus, for $k = 1$, the $\beta_{k-1}q_{k-1}$ term is set to $\beta_0 q_0 = 0$. Now the columns of Q can be built by iterating from $k = 1$ to $k = n$.

B.1.3 Algorithm

1. Set $r_0 = q_1$,$\beta_0 = 1$ and $q_0 = 0$
2. For k=1,2,3,...,n:
3. $q_{k+1} = \frac{r_k}{\beta_k}$
4. $\alpha_k = q_k^T A q_k$
5. $r_k = (A - \alpha_k I)q_k - \beta_{k-1}q_{k-1}$
6. $\beta_k = ||r_k||_2$
7. Reorthonormalize $\{q_i\}_{i=1}^k$ if necessary
8. Approximate Eigenvalues and Eigenvectors (Can be done after the loop instead)

Line 1: β_0 is set to 1 since it is the norm of r_0 and $r_0 = q_1$, where q_1 is a normalized vector.

Line 2: The for loop runs from $k = 1$ all the way up to $k = n$, where n is the total number of columns. Depending of the eigenvalues desired, this loop can instead be a while loop that ends whenever the eigenvalues have reached a desired tolerance.

Line 7: Due to finite precision errors, the set of supposedly mutually orthonormal vectors $\{q_i\}_{i=1}^{k}$ will actually lose their orthonormality at later Lanczos steps. When this happens, a reorthonormalization scheme, such as the Grahm-Schmidt Process, has to be employed.

Line 8: Again, depending on the problem and the desired eigenpairs, the approximation can be done for the current version of the tridiagonal matrix at step k, call it T_k. Alternatively, it could be done after the for loop has finished and the full tridiagonal matrix has been T built. There is no strict requirement on which iterative method should be used to find the eigendecomposition (QR Method, Power Iteration, Inverse Power Iteration, etc...).

B.1.4 Code

An implementation of the Lanczos Algorithm in Python can be found in: https://github.com/ecasiano/LanczosEigensolvers/blob/master/lanczosEigensolver.py. The code generates a random, sparse, hermitian matrix of specified size, finds a tridiagonal representation via Lanczos and calculates the full eigendecomposition via QR Algorithm or finds the smallest eigenvalue via Inverse Power Iteration. A blackbox function, part of the numpy.linalg package, numpy.linalg.eigsh(), solves the eigenvalue problem for the input matrix so a comparison can be made with the code results.

B.1.5 Results

The following colormap represents a sparse and hermitian matrix of dimensions $n \times n$ that was fed to the linked Lanczos code. The Lanczos iterations were

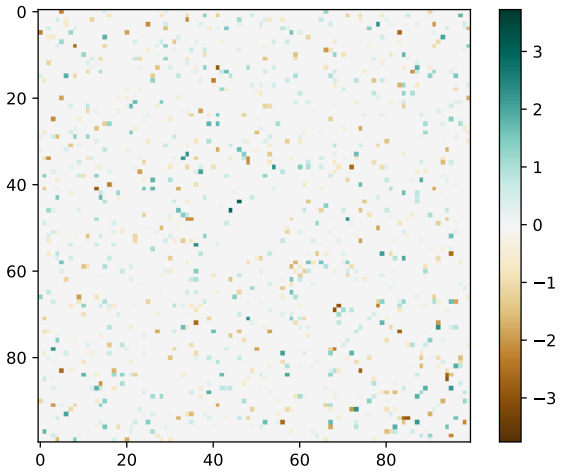

Figure B.1: Colormap representing a randomly generated sparse hermitian matrix to be diagonalized via Lanczos iteration. The zero entries are denoted by gray squares.

carried from $k = 1$ to $k = n = 100$. First, Lanczos was ran without reorthonormalizing the columns of the transform matrix Q. Observe in Figure B.2 how the matrix starts to look tridiagonal, but still has some large nonzero entries far away from the diagonal. This is the result of finite precision error. Via the Grahm-Schmidt Procedure, a full reorthonormalization was then done at each Lanczos step. Figure B.3 shows the resulting matrix after reorthonormalization was done at every iteration. Barring some small nonzero entries in the bottom right, most likely due also to finite precision, the matrix was now tridiagonalized successfully.

Figure B.4 shows the eigenvalues obtained using the Lanczos code linked and those obtained using numpy.linalg.eigsh function. These eigenvalues correspond to the same matrix generated for the plots in the previous section.

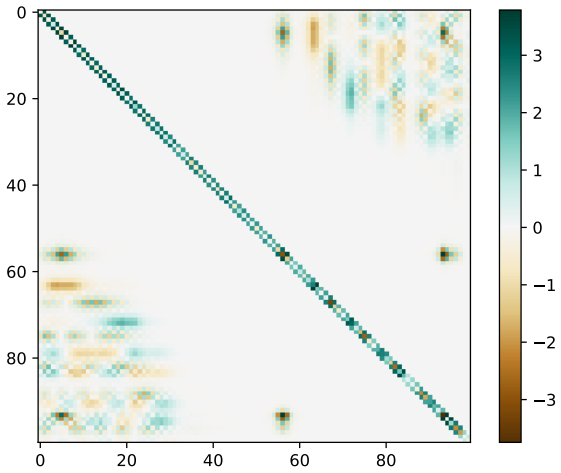

Figure B.2: Colormap representing the matrix after 100 steps of Lanczos iterations have been done. Due to normalization being lost at each iteration, there are still large off diagonal entries.

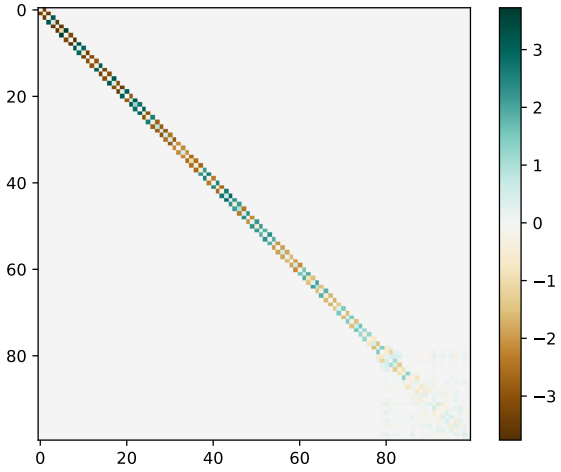

Figure B.3: Colormap representing the matrix after 100 steps of Lanczos iterations with reorthonormalization have been done. Note that off-diagonal elements are almost all non-zero, besides some very small entries in the bottom right due to numerical precision errors.

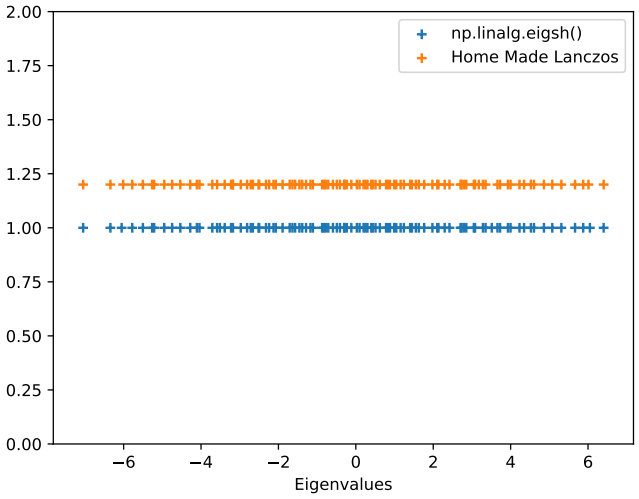

Figure B.4: Scatter plot comparing the eigenvalues obtained with my implementation of the code and with a numpy implementation. The vertical axis carries no significance and values have been shifted in order to make the comparison easier. The horizontal axis shows the actual eigenvalues obtained. Agreement is seen between both of the implementations.

Appendix C

C.1 Evaluating the n-particle partition entanglement

In this appendix, we show that the n-RDM of spinless hardcore particles on a lattice can be written as a tensor product of two lower-rank matrices. This simplification significantly reduces the numerical cost for calculating n-RDM for such quantum systems.

In general, for a pure quantum state $|\Psi\rangle$ in some Hilbert space $\mathcal{H}$ that can be written as the tensor product space $A \otimes B$, we can write

$$|\Psi\rangle = \sum_{i,j} C_{i,j} |\psi_i^A\rangle |\psi_j^B\rangle, \tag{C.1}$$

where $\{|\psi_i^A\rangle\}$ and $\{|\psi_j^B\rangle\}$ are orthonormal bases in the two Hilbert spaces A and B, respectively. Accordingly, the system degrees of freedom are bipartitioned between the two subsets $\{|\psi_i^A\rangle\}$ and $\{|\psi_j^B\rangle\}$. Using the product basis $\{|\psi_i^A\rangle|\psi_j^B\rangle\}$, the full density matrix can be written as

$$\rho = |\Psi\rangle\langle\Psi| = \sum_{i,j,i',j'} |\psi_i^A\rangle|\psi_j^B\rangle C_{i,j} C^*_{i',j'} \langle\psi_{i'}^A|\langle\psi_{j'}^B|. \tag{C.2}$$

The reduced density matrix ρ_A (ρ_B) of subspace A (B) , is obtained from ρ by

tracing out the degrees of freedom of subspace B (A),

$$\rho_A = \sum_m \langle \psi_m^B | \rho | \psi_m^B \rangle = \sum_{i,j} |\psi_i^A\rangle \left(\sum_m C_{i,m} C_{j,m}^* \right) \langle \psi_j^A |, \tag{C.3}$$

$$\rho_B = \sum_m \langle \psi_m^A | \rho | \psi_m^A \rangle = \sum_{i,j} |\psi_i^B\rangle \left(\sum_m C_{m,i} C_{m,j}^* \right) \langle \psi_j^B |. \tag{C.4}$$

Moreover, the reduced density matrices can be generated using the linear maps $G_{AB} : S_B \to S_A$ as $\rho_A = G_{AB} G_{AB}^\dagger$ and $\rho_B = (G_{AB}^\dagger G_{AB})^T$ where

$$G_{AB} = \sum_{i,j} C_{i,j} |\psi_i^A\rangle \langle \psi_j^B |. \tag{C.5}$$

Note that, in general, the matrix representing the linear maps G_{AB} is rectangular since the dimensions of the Hilbert spaces A and B can differ.

C.1.1 Particle bipartition

Let us now consider a quantum system of N spinless hardcore particles in a state $|\Psi\rangle = \sum_i \chi_i |\psi_i^N\rangle$, where $\{|\psi_i^N\rangle\}$ are the N particle second-quantization basis states, where each basis state corresponds to a single, possible, occupation number configuration (ONC). Now we recall that each ONC state is a linear combination of the distinguished particles states $\{|\psi_{i,j}^N\rangle\}$ as $|\psi_i^N\rangle = \sum_j \frac{f_j}{\sqrt{N!}} |\psi_{i,j}^N\rangle$, where j runs over all possible particle permutations (PPs) and $f_j = e^{-i\phi_j}$ is the corresponding phase factor. Accordingly, we can write

$$|\Psi\rangle = \sum_{i,j} \frac{\chi_i f_j}{\sqrt{N!}} |\psi_{i,j}^N\rangle. \tag{C.6}$$

Now we partition N into two sets of particles: n_A and the remainder $n_B = N - n_A$. The distinguished particles basis $\{|\psi_{i,j}^N\rangle\}$ can be written as a tensor

product of the two partitions basis

$$|\psi^N_{i,j}\rangle = |\psi^{n_A}_{i_A,j_A}\rangle|\psi^{n_B}_{i_B,j_B}\rangle, \tag{C.7}$$

where each ONC (labelled by i) of the N particles corresponds to a unique pair of ONCs i_A and i_B of the n_A and n_B particles, respectively. Similarly, each PP j of the N particles corresponds to a unique pair of PPs: j_A and j_B of the n_A and n_B particles.

$$|\Psi\rangle = \sum_{i_A,i_B,j_A,j_B} C_{i_A,i_B,j_A,j_B}|\psi^{n_A}_{i_A,j_A}\rangle|\psi^{n_B}_{i_B,j_B}\rangle, \tag{C.8}$$

with

$$C_{i_A,i_B,j_A,j_B} = \frac{\chi_i f_j}{\sqrt{N!}}. \tag{C.9}$$

The C_{i_A,i_B,j_A,j_B} depends on the indices i and j through the multiplication of χ_i and f_j, and without loss of generality, we can take

$$C_{i_A,i_B,j_A,j_B} = \tilde{C}_{i_A,i_B}\Phi_{j_A,j_B}. \tag{C.10}$$

Moreover, the dependence of Φ_{j_A,j_B} on the PP indices only guarantees that $|\Phi_{j_A,j_B}|^2 = \textit{constant}$ that can be absorbed in $\tilde{C}_{i_A,i_B}$. Thus, we can set $|\Phi_{j_A,j_B}|^2 = 1$. Based on the fact that applying a particle permutation two one group of particles results in an overall phase factor that does not depend on the permutation of the other group of particles, we write

$$\Phi_{j_A,j_B} = F^{(A)}_{j_A}F^{(B)}_{j_B}, \tag{C.11}$$

with $|F^{(A)}_{j_A}|^2 = |F^{(B)}_{j_B}|^2 = 1$. Substituting in Eq. (C.8) we find

$$|\Psi\rangle = \sum_{i_A,i_B,j_A,j_B} \tilde{C}_{i_A,i_B}F^{(A)}_{j_A}F^{(B)}_{j_B}|\psi^{n_A}_{i_A,j_A}\rangle|\psi^{n_B}_{i_B,j_B}\rangle, \tag{C.12}$$

Let us now calculate the reduced density matrix of ρ_A using

$$G_{n_A n_B} = \sum_{i_A, i_B, j_A, j_B} \tilde{C}_{i_A, i_B} F^{(A)}_{j_A} F^{(B)}_{j_B} |\psi^{n_A}_{i_A, j_A}\rangle\langle\psi^{n_B}_{i_B, j_B}|, \tag{C.13}$$

as

$$\begin{aligned}
\rho_A &= G_{n_A n_B} G^{\dagger}_{n_A n_B} && \text{(C.14)} \\
&= \sum_{i_A, j_A, i'_A, j'_A} |\psi^{n_A}_{i_A, j_A}\rangle \sum_{i_B} \left(\tilde{C}_{i_A, i_B} \tilde{C}^{*}_{i'_A, i_B} \right) F^{(A)}_{j_A} F^{*(A)}_{j'_A} \sum_{j_B} \left| F^{(B)}_{j_B} \right|^2 \langle\psi^{n_A}_{i'_A, j'_A}| \\
&= n_B! \sum_{i_A, j_A, i'_A, j'_A} |\psi^{n_A}_{i_A, j_A}\rangle D_{i_A, i'_A} \Phi_{j_A, j'_A} \langle\psi^{n_A}_{i'_A, j'_A}|, && \text{(C.15)}
\end{aligned}$$

with $D_{i_A, i'_A} = \sum_{i_B} \tilde{C}_{i_A, i_B} \tilde{C}^{*}_{i'_A, i_B}$ and $\Phi_{j_A, j'_A} = F^{(A)}_{j_A} F^{*(A)}_{j'_A}$. From Eq. (C.15) we see that ρ_A is a Kronecker product (tensor product) of the lower-rank Hermitian matrices D and Φ. where D can be calculated considering a single PP for each particle partition and the elements of Φ are the product of the relative phases of the chosen partitions (C.11)

C.1.2 Eigenvalues

Let V_D and V_Φ be two unitary transformations that diagonalize the sub matrices D and Φ, respectively. Such that $V^{\dagger}_D D V_D = \Lambda$ and $V^{\dagger}_\Phi \Phi V_\Phi = W$, where Λ and W are diagonal matrices with eigenvalues $\{\lambda_k\}$ and $\{w_l\}$. If we construct the unitary transformation U as

$$U = V_D \otimes V_\Phi, \tag{C.16}$$

and calculate $U^{\dagger}(\rho_A / n_B!)U$ we find

$$U^{\dagger} \left(\frac{\rho_A}{n_B!} \right) U = \sum_{k,l} |\psi^{n_1}_{k,l}\rangle \lambda_k w_l \langle\psi^{n_1}_{k,l}|. \tag{C.17}$$

Accordingly, the unitary transformation U diagonalizes ρ_A and the eigenvalues of ρ_A are $n_B!\lambda_k w_l$. Moreover, Φ has the structure of a simple projection operator onto the non-normalized state $|F^{(A)}\rangle = \sum_j^{n_A!} F_j^{(A)}|j\rangle = \sum_j^{n_A!} e^{i\phi_j}|j\rangle$ as $\Phi = |F^{(A)}\rangle\langle F^{(A)}|$. The only eigenstate of Φ with a nonzero eigenvalue is $|F^{(A)}\rangle$, where $\Phi|F^{(A)}\rangle = |F^{(A)}\rangle\langle F^{(A)}|F^{(A)}\rangle = n_A!|F^{(A)}\rangle$.

Therefore, we conclude that the nonzero eigenvalues of ρ_A are $n_A!n_B!\lambda_k$, where λ_k are the eigenvalues of the matrix D that is constructed using only one PP of each of the sets $\{|\psi^{n_A}_{i_A,j_A}\rangle\}$ and $\{|\psi^{n_B}_{i_B,j_B}\rangle\}$. As the rank of D is smaller than that of the n-RDM by a factor of $n_A!n_B!$ the numerical effort involved in calculating the eigenvalues of the n-RDM is enormously reduced.

C.2 n-particle partition entanglement in the $V/t \to \infty$ limit

Here we calculate the n-particle partition entanglement of the one-dimensional fermionic $t-V$ model at half filling ($N = M/2$) in the infinite repulsion limit ($V/t \to \infty$). In this limit, the Hamiltonian of the model (Eq. (2.18)) is reduced to

$$H = V \sum_i n_i n_{i+1} \tag{C.18}$$

which is diagonal in the occupation number representation with a two-fold degenerate ground state, where, at half filling, the fermions can avoid having any nearest neighbors by occupying sites with only odd indices ($|\psi_{\text{odd}}\rangle = |1010\cdots10\rangle$) or only even indices ($|\psi_{\text{even}}\rangle = |0101\cdots01\rangle$). Thus, one can write the ground state in this limit, as a superposition of $|\psi_{\text{odd}}\rangle$ and $|\psi_{\text{even}}\rangle$:

$$|\Psi\rangle = \cos(\Theta)e^{i\delta}|\psi_{\text{odd}}\rangle + \sin(\Theta)|\psi_{\text{even}}\rangle, \tag{C.19}$$

where we parametrize the amplitudes and the relative phase of the odd/even states using Θ and δ. Note that for $\delta = 0$ and $\Theta = \pi/4$ ($\Theta = 3\pi/4$), the ground state $|\Psi\rangle$ is also an eigenstate of the inversion operator P (Eq. (2.22)) with eigenvalue ± 1 where

$$P|\Phi_\pm\rangle = \pm|\Phi_\pm\rangle = \pm\left(\frac{1}{\sqrt{2}}|\psi_{\text{odd}}\rangle \pm \frac{1}{\sqrt{2}}|\psi_{\text{even}}\rangle\right). \tag{C.20}$$

The degeneracy persists in the case of finite interaction V/t for even/odd N with PBC/APBC. The degeneracy is lifted for odd/even N with APBC/PBC with the resulting ground state in the infinite repulsion limit approaching an eigenstate of P:

$$|\Psi\rangle = |\Phi_+\rangle = \frac{1}{\sqrt{2}}|\psi_{\text{odd}}\rangle + \frac{1}{\sqrt{2}}|\psi_{\text{even}}\rangle. \tag{C.21}$$

We now consider the n-particle partition entanglement of the degenerate ground state $|\Psi\rangle$ defined in Eq. (C.19), where we can write the corresponding full density matrix ρ as

$$\begin{aligned}\rho = &\cos^2(\Theta)|\psi_{\text{odd}}\rangle\langle\psi_{\text{odd}}| + \sin^2(\Theta)|\psi_{\text{even}}\rangle\langle\psi_{\text{even}}| \\ &+ \sin(\Theta)\cos(\Theta)e^{i\delta}|\psi_{\text{odd}}\rangle\langle\psi_{\text{even}}| + \sin(\Theta)\cos(\Theta)e^{-i\delta}|\psi_{\text{even}}\rangle\langle\psi_{\text{odd}}|,\end{aligned} \tag{C.22}$$

If we partition the N particles into two distinguishable sets of $n_A = n$ and $n_B = N - n$ particles, we can write the states $|\psi_{odd}\rangle$ and $|\psi_{even}\rangle$ in terms of the first-quantized basis states of the two partitions as

$$|\psi_{\text{odd}}\rangle = \sum_{i_A,i_B,j_A,j_B} \frac{f^{\text{odd}}_{i_A,i_B,j_A,j_B}}{\sqrt{N!}}|\psi^{n_A,\text{odd}}_{i_A,j_A}\rangle|\psi^{n_B,\text{odd}}_{i_B,j_B}\rangle, \tag{C.23}$$

$$|\psi_{\text{even}}\rangle = \sum_{i_A,i_B,j_A,j_B} \frac{f^{\text{even}}_{i_A,i_B,j_A,j_B}}{\sqrt{N!}}|\psi^{n_A,\text{even}}_{i_A,j_A}\rangle|\psi^{n_B,\text{even}}_{i_B,j_B}\rangle, \tag{C.24}$$

where the indices i_A and i_B label possible occupation number configurations (ONCs) in both partitions A and B while j_A and j_B label different particle

permutations (PPs). Also, $f^{\text{odd}}_{i_A,i_B,j_A,j_B}$ and $f^{\text{even}}_{i_A,i_B,j_A,j_B}$ are overall phase factors, where the superscript odd (even) is to indicate that only sites with odd (even) indices are occupied. We note that in this decomposition the states $|\psi_{\text{even}}\rangle$ and $|\psi_{\text{odd}}\rangle$ are constructed from non-overlapping subspaces (even/odd) of partition B. Similarly for partition A. By tracing out all degrees of freedom in B from ρ (Eq. (C.22)), we can write the reduced density matrix ρ_A as

$$\rho_A = \text{Tr}_B\, \rho = \cos^2(\Theta)\text{Tr}_B\, |\psi_{\text{odd}}\rangle\langle\psi_{\text{odd}}| + \sin^2(\Theta)\text{Tr}_B\, |\psi_{\text{even}}\rangle\langle\psi_{\text{even}}|, \qquad \text{(C.25)}$$

where the trace of the mixed terms ($|\psi_{\text{odd}}\rangle\langle\psi_{\text{even}}|$, $|\psi_{\text{even}}\rangle\langle\psi_{\text{odd}}|$) vanishes due to the non-sharing of B basis states. Moreover, $\rho_A^{\text{odd}} = \text{Tr}_B\, |\psi_{\text{odd}}\rangle\langle\psi_{\text{odd}}|$ and $\rho_A^{\text{even}} = \text{Tr}_B\, |\psi_{\text{even}}\rangle\langle\psi_{\text{even}}|$ contribute separately to the spectrum of ρ_A due to the non-sharing of A basis states.

We now calculate the spectrum of ρ_A^{odd}. Note that the state $|\psi_{\text{odd}}\rangle$ represents a single ONC of the N particles and as a result the ONC i_A is uniquely determined by i_B in the product states $|\psi^{n_A,\text{odd}}_{i_A,j_A}\rangle|\psi^{n_B,\text{odd}}_{i_B,j_B}\rangle$. Therefore, ρ_A^{odd} does not connect any pair of states, in the set $\{|\psi^{n_A,\text{odd}}_{i_A,j_A}\rangle\}$, with different ONC i_A. This result, allows us to identify that the sector of ρ_A^{odd} that connects states in $\{|\psi^{n_A,\text{odd}}_{i_A,j_A}\rangle\}$ with fixed PP j_A is diagonal with $\binom{N}{n}$ equal non-zero elements of value $\frac{1}{N!}$. $\binom{N}{n}$ is the number of possible ONCs in the partition A with $n_A = n$ and we only consider the contribution of a single PP j_B to $\text{Tr}_B\, |\psi_{\text{odd}}\rangle\langle\psi_{\text{odd}}|$. It then follows from **??** that the non-zero eigenvalues of ρ_A^{odd} can be obtained by rescaling the above eigenvalues by a factor of $n_A!n_B! = n!(N-n)!$. By an equivalent set of arguments ρ_A^{even} has the same eigenvalues. Combining all the above and using Eq. (C.25), we find that ρ_A has two sets of eigenvalues: $\binom{N}{n}$ eigenvalues of $\cos^2(\Theta)/\binom{N}{n}$ and $\binom{N}{n}$ eigenvalues of $\sin^2(\Theta)/\binom{N}{n}$. Therefore, the Rényi entanglement entropies are

$$S_\alpha(n) = \ln\binom{N}{n} + \frac{1}{1-\alpha}\ln\left[\cos^{2\alpha}(\Theta) + \sin^{2\alpha}(\Theta)\right], \qquad \text{(C.26)}$$

and the von Neumann entropy ($\alpha = 1$) is

$$S_1(n) = \ln \binom{N}{n} - \cos^2(\Theta) \ln \left[\cos^2(\Theta)\right] - \sin^2(\Theta) \ln \left[\sin^2(\Theta)\right]. \tag{C.27}$$

According to Eqs. (C.26) and (C.27), the maximum entropy corresponds to $\Theta = \pi/4$ and $3\pi/4$ ($|\Psi\rangle = \frac{e^{i\delta}}{\sqrt{2}}|\psi_{\text{odd}}\rangle + \frac{1}{\sqrt{2}}|\psi_{\text{even}}\rangle$), where all the $2\binom{N}{n}$ eigenvalues of ρ_A are equal and thus all the Rényi entropies are equal to

$$S_\alpha(n) = \ln \binom{N}{n} + \ln 2. \tag{C.28}$$

For $\Theta = 0$ and $\pi/2$, $|\Psi\rangle = |\psi_{\text{odd}}\rangle$ or $|\psi_{\text{even}}\rangle$, only $\binom{N}{n}$ equal eigenvalues survive yielding a minimum entropy of

$$S_\alpha(n) = \ln \binom{N}{n}. \tag{C.29}$$

These limits can be seen in Fig. 2.6 for $V/t \gg 1$.

Appendix D

D.1 Ground state of the $t-V$ model for $V/t = -2$

Consider the Hamiltonian of the $t - V$ model given in Eq. 1.1 at the special interaction strength $V = -2t$ corresponding to the first order phase transition:

$$H = -t\sum_{i=1}^{L}(c_i^\dagger c_{i+1} + c_{i+1}^\dagger c_i) - 2t\sum_{i=1}^{L} n_i n_{i+1} \tag{D.1}$$

where we assume periodic boundary conditions for N even and anti-periodic boundary conditions for N odd.

D.1.1 Fermion occupation basis

We study the effect of H in the N fermion occupation basis $\{|\psi_a\rangle\}$, where the index a runs over all of the $\binom{L}{N}$ possible configurations. For example, for $N = 2$ and $L = 4$ there are six such states: $|\psi_a\rangle \in \{|1100\rangle, |1010\rangle, |1001\rangle, |0110\rangle, |0101\rangle, |0011\rangle\}$.

Starting with the potential operator $\mathcal{V} \equiv -2t\sum_{i=1}^{L} n_i n_{i+1}$ which is diagonal in this basis, we have

$$\mathcal{V}\,|\psi_a\rangle = -2t\, n_a^{(11)}\,|\psi_a\rangle\ , \tag{D.2}$$

where $n_a^{(11)}$ counts the number of bonds connecting two occupied sites in the state $|\psi_a\rangle$. The hopping operator $\mathcal{T} \equiv -t\sum_{i=1}^{L}(c_i^\dagger c_{i+1} + c_{i+1}^\dagger c_i)$ turns $|\psi_a\rangle$ into a superposition of all the states $|\psi_b\rangle$ connected to $|\psi_a\rangle$ by moving one particle

to a neighboring empty site. We can write:

$$\mathcal{T}\,|\psi_a\rangle = -t \sum_{b\in \mathsf{S}_a} |\psi_b\rangle \ , \tag{D.3}$$

where S_a is the resulting index set of occupation states $|\psi_b\rangle$, i.e. $b \in \mathsf{S}_a \iff \langle\psi_b|\mathcal{T}|\psi_a\rangle \neq 0$. The cardinality of S_a is

$$\begin{aligned} \mathrm{card}(\mathsf{S}_a) &\equiv \sum_{b\in \mathsf{S}_a} 1 \\ &= n_a^{(10)} + n_a^{(01)} \\ &= 2N - 2n_a^{(11)}, \end{aligned} \tag{D.4}$$

where $n_a^{(10)}$ ($n_a^{(01)}$) counts the number of occupied-empty (empty-occupied) bonds in $|\psi_a\rangle$ and in the last line we have used the fact that the total number of particles on a ring is (independent of the index a)

$$N = n_a^{(11)} + (n_a^{(10)} + n_a^{(01)})/2. \tag{D.5}$$

A general matrix element in the fermion occupation basis is given by:

$$\langle\psi_c|\mathcal{T}|\psi_a\rangle = -t \begin{cases} 1 & c \in \mathsf{S}_a \\ 0 & \text{otherwise} \end{cases} \tag{D.6}$$

which is guaranteed to be real, thus

$$\langle\psi_c|\mathcal{T}|\psi_a\rangle = \langle\psi_a|\mathcal{T}|\psi_c\rangle \Rightarrow c \in \mathsf{S}_a \iff a \in \mathsf{S}_c. \tag{D.7}$$

This is a useful result that can be used to swap the order of restricted and un-restricted summations.

Let us know consider the action of $\mathcal{T}$ on a general state $|\Psi\rangle = \sum_a \mathcal{C}_a\,|\psi_a\rangle$

where $\mathcal{C}_a \in \mathbb{C}$:

$$\begin{aligned}\mathcal{T}\,|\Psi\rangle &= -t\sum_a \mathcal{C}_a \sum_{b\in \mathsf{S}_a} |\psi_b\rangle \\ &= -t\sum_c |\psi_c\rangle \sum_a \mathcal{C}_a \sum_{b\in \mathsf{S}_a} \langle\psi_c|\psi_b\rangle \\ &= -t\sum_c |\psi_c\rangle \left[\sum_a \mathcal{C}_a \sum_{b\in \mathsf{S}_a} \delta_{c,b}\right] \end{aligned} \tag{D.8}$$

where we have inserted a resolution of the identity operator $\sum_c |\psi_c\rangle \langle\psi_c| = \mathbb{1}$ into the second line. Now, $\sum_{b\in \mathsf{S}_a} \delta_{c,b} \neq 0 \iff c \in \mathsf{S}_a$ and using Eq. (D.7) we can write

$$\sum_a \mathcal{C}_a \sum_{b\in \mathsf{S}_a} \delta_{c,b} = \sum_{a\in S_c} \mathcal{C}_a\,. \tag{D.9}$$

Substituting into Eq D.8 above and relabelling $a \leftrightarrow c$ leads to the general result:

$$\mathcal{T}\,|\Psi\rangle = -t\sum_a \sum_{c\in \mathsf{S}_a} \mathcal{C}_c\,|\psi_a\rangle\,. \tag{D.10}$$

Written in this form, we can combine Eq. (D.10) with Eqs. (D.2) and (D.4) to compute the action of the full Hamiltonian at $V = -2t$ on $|\Psi\rangle$:

$$\begin{aligned} H\,|\Psi\rangle &= -t\sum_a \left[\sum_{c\in \mathsf{S}_a} \mathcal{C}_c + 2n_a^{(11)}\mathcal{C}_a\right] |\psi_a\rangle \\ &= -2tN\,|\Psi\rangle - t\sum_a \sum_{c\in \mathsf{S}_a} (\mathcal{C}_c - \mathcal{C}_a)\,|\psi_a\rangle\ . \end{aligned} \tag{D.11}$$

D.1.2 The Flat State

From Eq. (D.11) it is immediately apparent that the flat state

$$|\Psi_0\rangle = \frac{1}{\sqrt{\binom{L}{N}}} \sum_a |\psi_a\rangle \tag{D.12}$$

is an eigenstate of H with energy $-2tN$. To prove that $|\Psi_0\rangle$ is indeed the ground state, we consider matrix elements of the shifted operator $H' = H + 2tN$ for a

general state $|\Psi\rangle$ expanded in the fermion occupation basis:

$$\begin{aligned}\langle\Psi|H'|\Psi\rangle &= -t\sum_{a,b}\sum_{c\in\mathsf{S}_a}\left(\mathcal{C}_c-\mathcal{C}_a\right)\langle\psi_b|\psi_a\rangle\,\mathcal{C}_b^* \\ &= t\sum_{a}\sum_{c\in\mathsf{S}_a}\left(|\mathcal{C}_a|^2-\mathcal{C}_a^*\mathcal{C}_c\right) \\ &= t\sum_{a}\sum_{c\in\mathsf{S}_a}\left(|\mathcal{C}_c|^2-\mathcal{C}_c^*\mathcal{C}_a\right) \qquad \text{(D.13)}\end{aligned}$$

where we have swapped the summations (and relabelled) in the last line making use of Eq. (D.7). Now, we can rewrite the matrix element as:

$$\begin{aligned}\langle\Psi|H'|\Psi\rangle &= \frac{t}{2}\sum_{a}\sum_{c\in\mathsf{S}_a}\left(|\mathcal{C}_a|^2-\mathcal{C}_a^*\mathcal{C}_c+|\mathcal{C}_c|^2-\mathcal{C}_c^*\mathcal{C}_a\right) \\ &= \frac{t}{2}\sum_{a}\sum_{c\in\mathsf{S}_a}|\mathcal{C}_a-\mathcal{C}_c|^2\geq 0. \qquad \text{(D.14)}\end{aligned}$$

Thus H' is a positive operator and the flat state $|\Psi_0\rangle$ is the ground state of H at $V=-2t$ for fixed N.

Bibliography

[1] M. B. Hastings, I. González, A. B. Kallin, and R. G. Melko. "Measuring Renyi Entanglement Entropy in Quantum Monte Carlo Simulations." Phys. Rev. Lett. **104**, 157201 (2010).

[2] R. Islam, R. Ma, P. M. Preiss, M. E. Tai, A. Lukin, M. Rispoli, and M. Greiner. "Measuring entanglement entropy in a quantum many-body system." Nature **528**, 77 (2015).

[3] H. M. Wiseman and J. A. Vaccaro. "Entanglement of Indistinguishable Particles Shared between Two Parties." Phys. Rev. Lett. **91**, 097902 (2003).

[4] H. Barghathi, C. M. Herdman, and A. Del Maestro. "Rényi Generalization of the Accessible Entanglement Entropy." Phys. Rev. Lett. **121** (2018). `http://dx.doi.org/10.1103/PhysRevLett.121.150501`

[5] P. Zanardi. "Virtual Quantum Subsystems." Phys. Rev. Lett. **87**, 077901 (2001).

[6] Y. Shi. "Quantum entanglement of identical particles." Phys. Rev. A **67**, 024301 (2003).

[7] Y. Shi. "Quantum entanglement in second-quantized condensed matter systems." J. Phys. A: Math. Gen **37**, 6807 (2004).

[8] G. Ghirardi and L. Marinatto. "General criterion for the entanglement of two indistinguishable particles." Phys. Rev. A **70**, 012109 (2004).

[9] H. Barnum, E. Knill, G. Ortiz, R. Somma, and L. Viola. "A Subsystem-Independent Generalization of Entanglement." Phys. Rev. Lett. **92**, 107902 (2004).

[10] J. Dunningham, A. Rau, and K. Burnett. "From Pedigree Cats to Fluffy-Bunnies." Science **307**, 872 (2005).

[11] H. M. Wiseman, S. D. Bartlett, and J. A. Vaccaro. "Ferreting out the fluffy bunnies: entanglement constrained by generalized superselection rules." In "Proceedings of the XVI International Conference on Laser Spectroscopy," pages 307–314 (World Scientific, Queensland, Australia, 2011).
https://www.worldscientific.com/doi/abs/10.1142/9789812703002_0047

[12] F. Benatti, R. Floreanini, and U. Marzolino. "Entanglement robustness and geometry in systems of identical particles." Phys. Rev. A **85**, 042329 (2012).

[13] A. P. Balachandran, T. R. Govindarajan, A. R. de Queiroz, and A. F. Reyes-Lega. "Entanglement and Particle Identity: A Unifying Approach." Phys. Rev. Lett. **110**, 080503 (2013).

[14] B. J. Dalton, J. Goold, B. M. Garraway, and M. D. Reid. "Quantum entanglement for systems of identical bosons: I. general features." Phys. Scrip. **92**, 023004 (2017).

[15] C. Simon. "Natural entanglement in Bose-Einstein condensates." Phys. Rev. A **66**, 052323 (2002).

[16] W. Ding and K. Yang. "Entanglement entropy and mutual information in Bose-Einstein condensates." Phys. Rev. A **80**, 012329 (2009).

[17] J. Schliemann, J. I. Cirac, M. Kuś, M. Lewenstein, and D. Loss. "Quantum correlations in two-fermion systems." Phys. Rev. A **64**, 022303 (2001).

[18] P. Zanardi. "Quantum entanglement in fermionic lattices." Phys. Rev. A **65**, 042101 (2002).

[19] P. Zanardi and X. Wang. "Fermionic entanglement in itinerant systems." J. Phys. A: Math. and Gen. **35**, 7947 (2002).

[20] M. C. Tichy, F. Mintert, and A. Buchleitner. "Essential entanglement for atomic and molecular physics." J. Phys. B: Atom., Mol. and Opt. Phys. **44**, 192001 (2011).

[21] N. Killoran, M. Cramer, and M. B. Plenio. "Extracting entanglement from identical particles." Phys. Rev. Lett. **112**, 150501 (2014).

[22] O. S. Zozulya, M. Haque, K. Schoutens, and E. H. Rezayi. "Bipartite entanglement entropy in fractional quantum Hall states." Phys. Rev. B **76**, 125310 (2007).

[23] M. Haque, O. Zozulya, and K. Schoutens. "Entanglement Entropy in Fermionic Laughlin States." Phys. Rev. Lett. **98**, 060401 (2007).

[24] O. Zozulya, M. Haque, and K. Schoutens. "Particle partitioning entanglement in itinerant many-particle systems." Phys. Rev. A **78**, 042326 (2008).

[25] M. Haque, O. S. Zozulya, and K. Schoutens. "Entanglement between particle partitions in itinerant many-particle states." J. Phys. A: Math. Theor. **42**, 504012 (2009).

[26] H. Katsura and Y. Hatsuda. "Entanglement entropy in the Calogero-Sutherland model." J. Phys. A: Math. Theor. **40**, 13931 (2007).

[27] R. Santachiara, F. Stauffer, and D. C. Cabra. "Entanglement properties and momentum distributions of hard-core anyons on a ring." J. Stat. Mech.: Theor. Exp. **2007**, L05003 (2007).

[28] C. M. Herdman, P. N. Roy, R. G. Melko, and A. Del Maestro. "Particle entanglement in continuum many-body systems via quantum Monte Carlo." Phys. Rev. B **89**, 140501 (2014).

[29] C. M. Herdman and A. Del Maestro. "Particle partition entanglement of bosonic Luttinger liquids." Phys. Rev. B **91**, 184507 (2015).

[30] Z. Liu and H. Fan. "Particle entanglement in rotating gases." Phys. Rev. A **81**, 062302 (2010).

[31] P. Calabrese and J. Cardy. "Entanglement entropy and quantum field theory." J. Stat. Mech.: Theor. Exp. **2004**, P06002 (2004).

[32] P. Calabrese, M. Mintchev, and E. Vicari. "Entanglement Entropy of One-Dimensional Gases." Phys. Rev. Lett. **107** (2011).

[33] P. Calabrese, M. Mintchev, and E. Vicari. "The entanglement entropy of one-dimensional systems in continuous and homogeneous space." J. Stat. Mech. Theor. Exp. **2011**, P09028 (2011).

[34] S.-I. Tomonaga. "Remarks on Bloch's Method of Sound Waves applied to Many-Fermion Problems." Prog. Theor. Phys. **5**, 544 (1951).

[35] F. D. M. Haldane. "Effective Harmonic-Fluid Approach to Low-Energy Properties of One-Dimensional Quantum Fluids." Phys. Rev. Lett. **47**, 1840 (1981).

[36] Barghathi, H and Casiano-Diaz, E and Del Maestro, A, 2017 GitHub Repository, `https://github.com/DelMaestroGroup/PartEntFermions` .

[37] T. Grover. "Entanglement of Interacting Fermions in Quantum Monte Carlo Calculations." Phys. Rev. Lett. **111**, 130402 (2013).

[38] J. McMinis and N. M. Tubman. "Renyi entropy of the interacting Fermi liquid." Phys. Rev. B **87**, 081108 (2013). `http://link.aps.org/doi/10.1103/PhysRevB.87.081108`

[39] J. E. Drut and W. J. Porter. "Hybrid Monte Carlo approach to the entanglement entropy of interacting fermions." Phys. Rev. B **92**, 125126 (2015). `https://link.aps.org/doi/10.1103/PhysRevB.92.125126`

[40] R. G. Melko, C. M. Herdman, D. Iouchtchenko, P. N. Roy, and A. Del Maestro. "Entangling qubit registers via many-body states of ultracold atoms." Phys. Rev. A **93**, 042336 (2016). `http://journals.aps.org/pra/abstract/10.1103/PhysRevA.93.042336`

[41] T. Giamarchi. *Quantum Physics in One Dimension* (Oxford University Press, Oxford, U.K., 2004).

[42] I. E. Dzyaloshinskii and A. I. Larkin. "Correlation functions for a one-dimensional Fermi system with long-range interaction (Tomonaga model)." Sov. Phys. JETP **38**, 202 (1974).

[43] M. A. Cazalilla. "Bosonizing one-dimensional cold atomic gases." J. Phys. B: At. Mol. Opt. Phys. **37**, S1 (2004).

[44] P. Jordan and E. Wigner. "Über das paulische äquivalenzverbot." Zeitschrift für Physik **47**, 631 (1928).

[45] J. D. Cloizeaux. "A soluble fermi-gas model. validity of transformations of the bogoliubov type." J. Math. Phys. **7**, 2136 (1966).

[46] J. D. Cloizeaux and M. Gaudin. "Anisotropic linear magnetic chain." J. Math. Phys. **7**, 1384 (1966).

[47] A. P. Kampf, M. Sekania, G. I. Japaridze, and P. Brune. "Nature of the insulating phases in the half-filled ionic hubbard model." J. Phys. Condens. Matter **15**, 5895 (2003).

[48] J. E. Drut and W. J. Porter. "Entanglement, noise, and the cumulant expansion." Phys. Rev. E **93**, 043301 (2016).

[49] W. J. Porter and J. E. Drut. "Entanglement spectrum and Rényi entropies of nonrelativistic conformal fermions." Phys. Rev. B **94**, 165112 (2016).

[50] I. Klich and L. S. Levitov. "Scaling of entanglement entropy and superselection rules." (2008).

[51] S. Humeniuk and T. Roscilde. "Quantum Monte Carlo calculation of entanglement Rényi entropies for generic quantum systems." Phys. Rev. B **86**, 235116 (2012).
http://link.aps.org/doi/10.1103/PhysRevB.86.235116

[52] C. M. Herdman, S. Inglis, P. N. Roy, R. G. Melko, and A. Del Maestro. "Path-integral Monte Carlo method for Rényi entanglement entropies." Phys. Rev. E **90**, 013308 (2014).

[53] A. J. Daley, H. Pichler, J. Schachenmayer, and P. Zoller. "Measuring Entanglement Growth in Quench Dynamics of Bosons in an Optical Lattice." Phys. Rev. Lett. **109**, 020505 (2012).

[54] A. M. Kaufman, M. E. Tai, A. Lukin, M. Rispoli, R. Schittko, P. M. Preiss, and M. Greiner. "Quantum thermalization through entanglement in an isolated many-body system." Science **353**, 794 (2016).
http://www.sciencemag.org/cgi/doi/10.1126/science.aaf6725

[55] H. Pichler, G. Zhu, A. Seif, P. Zoller, and M. Hafezi. "Measurement Protocol for the Entanglement Spectrum of Cold Atoms." Phys. Rev. X **6**, 041033 (2016).
http://link.aps.org/doi/10.1103/PhysRevX.6.041033

[56] N. M. Linke, S. Johri, C. Figgatt, K. A. Landsman, A. Y. Matsuura, and C. Monroe. "Measuring the Renyi entropy of a two-site Fermi-Hubbard model on a trapped ion quantum computer." (2017).
https://arxiv.org/abs/1712.08581

[57] A. Lukin, M. Rispoli, R. Schittko, M. E. Tai, A. M. Kaufman, S. Choi, V. Khemani, J. Léonard, and M. Greiner. "Probing entanglement in a many-body-localized system." (2018).
https://arxiv.org/abs/1805.09819

[58] C. Cachin. *Entropy Measures and Unconditional Security in Cryptography.* Ph.D. thesis, Swiss Federal Inst. Technol. (1997).

[59] L. Golshani, E. Pasha, and G. Yari. "Some properties of rényi entropy and rényi entropy rate." Inform. Sciences **179**, 2426 (2009). Including Special Section – Linguistic Decision Making.
http://www.sciencedirect.com/science/article/pii/S0020025509001145

[60] M. Hayashi. "Exponential decreasing rate of leaked information in universal random privacy amplification." IEEE T. Inform. Theory **57**, 3989 (2011).

[61] B. Škorić, C. Obi, E. Verbitskiy, and B. Schoenmakers. "Sharp lower bounds on the extractable randomness from non-uniform sources." Inform. Comput. **209**, 1184 (2011).
http://www.sciencedirect.com/science/article/pii/S0890540111000927

[62] S. Fehr and S. Berens. "On the Conditional Rényi Entropy." IEEE T. Inform. Theory **60**, 6801 (2014).

[63] U. Schollwöck. "The density-matrix renormalization group in the age of matrix product states." Annals of Physics **326**, 96 (2011). January 2011 Special Issue.
http://www.sciencedirect.com/science/article/pii/S0003491610001752

[64] (2018). Calculations performed using the ITensor C++ library (version 2.1.1), http://itensor.org/.

[65] IBM, 2019, IBM QuantumExperience, https://quantumexperience.ng.bluemix.net/qx.

[66] C. M. Herdman, P. N. Roy, R. G. Melko, and A. Del Maestro. "Spatial entanglement entropy in the ground state of the Lieb-Liniger model." Phys. Rev. B **94**, 064524 (2016).